Galaxy And Mass Assembly (GAMA): the effect of close interactions on star formation in galaxies

L. J. M. Davies,[1]★ A. S. G. Robotham,[1] S. P. Driver,[1,2] M. Alpaslan,[3] I. K. Baldry,[4]
J. Bland-Hawthorn,[5] S. Brough,[6] M. J. I. Brown,[7] M. E. Cluver,[8] M. J. Drinkwater,[9]
C. Foster,[6] M. W. Grootes,[10] I. S. Konstantopoulos,[6] M. A. Lara-López,[11]
Á. R. López-Sánchez,[6,12] J. Loveday,[13] M. J. Meyer,[1] A. J. Moffett,[1] P. Norberg,[14]
M. S. Owers,[6,12] C. C. Popescu,[15,16] R. De Propris,[17] R. Sharp,[18] R. J. Tuffs,[10]
L. Wang,[14,19] S. M. Wilkins,[13] L. Dunne,[20,21] N. Bourne[21] and M. W. L. Smith[22]

Affiliations are listed at the end of the paper

ABSTRACT

The modification of star formation (SF) in galaxy interactions is a complex process, with SF observed to be both enhanced in major mergers and suppressed in minor pair interactions. Such changes likely to arise on short time-scales and be directly related to the galaxy–galaxy interaction time. Here we investigate the link between dynamical phase and direct measures of SF on different time-scales for pair galaxies, targeting numerous star-formation rate (SFR) indicators and comparing to pair separation, individual galaxy mass and pair mass ratio. We split our sample into the higher (primary) and lower (secondary) mass galaxies in each pair and find that SF is indeed enhanced in all primary galaxies but suppressed in secondaries of minor mergers. We find that changes in SF of primaries are consistent in both major and minor mergers, suggesting that SF in the more massive galaxy is agnostic to pair mass ratio. We also find that SF is enhanced/suppressed more strongly for short-duration SFR indicators (e.g. Hα), highlighting recent changes to SF in these galaxies, which are likely to be induced by the interaction. We propose a scenario where the lower mass galaxy has its SF suppressed by gas heating or stripping, while the higher mass galaxy has its SF enhanced, potentially by tidal gas turbulence and shocks. This is consistent with the seemingly contradictory observations for both SF suppression and enhancement in close pairs.

Key words: galaxies: evolution – galaxies: interactions – galaxies: star formation.

1 INTRODUCTION

Interactions are a key process in the evolution of galaxies in the Universe (e.g. White & Frenk 1991). As galaxies interact and merge hierarchically over cosmic time-scales, these interaction events leave strong imprints on the galaxies involved, modifying their morphology (e.g. Conselice et al. 2003; Conselice, Black-burne & Papovich 2005; Lotz et al. 2008a,b; Mortlock et al. 2013, or see review in Conselice 2014), triggering active galactic nuclei (AGN; e.g. Kazantzidis et al. 2005; Hopkins et al. 2008; Medling et al. 2013, however cf. Villforth et al. 2014), varying gas fractions (e.g. Kazantzidis et al. 2005; Lotz et al. 2010; Ueda et al. 2012, 2013) and significantly altering their star formation (SF) history

(e.g. Di Matteo et al. 2007; Shi et al. 2009; Bournaud et al. 2011; Wong et al. 2011; Patton et al. 2013; Robotham et al. 2013). Such merger events are ubiquitous throughout the Universe, and as such probing the details of the merger process is key to our understanding of galaxy formation and evolution (e.g. Casteels et al. 2014). For example, SF initiated by interactions could well be a key factor in transforming blue star-forming discs into red, passively evolving quiescent spheroids.

However, the details of how SF responds to galaxy interactions are somewhat vague and are likely to be strongly linked to pair mass ratio and pair separation. Traditionally, observational studies of close pairs have highlighted strong evidence that SF is enhanced through interactions and that the strongest enhancement occurs in the closest pairs (those at projected separations of $<30\,$kpc; e.g. Ellison et al. 2008; Freedman Woods et al. 2010). In addition, detailed multi-wavelength analyses of blue compact dwarf galaxies

★ E-mail: luke.j.davies@uwa.edu.au

have shown that, in the majority of the cases, interactions with or between low-luminosity dwarf galaxies and H I clouds are the triggering mechanism of their strong SF activity (López-Sánchez 2010; López-Sánchez et al. 2012). More recently, Patton et al. (2013) have studied a large sample of star-forming galaxies in pairs taken from the Sloan Digital Sky Survey (SDSS) and found clear evidence for enhanced, emission line-derived SF out to significant pair separations (∼150 kpc). They also find that the enhancement in SF is inversely proportional to pair separation, with the closest pairs displaying the largest enhancement. This result is echoed by Wong et al. 2011 who perform a similar analysis for isolated pair galaxies in the PRIsm MUlti-object Survey (PRIMUS) but determine star formation rates (SFRs) using attenuation-corrected ultraviolet (UV)–optical colours. They find that pairs at separations of <50 kpc show bluer far-ultraviolet minus *r*-band (FUV−*r*) colours than a control sample of non-pair galaxies (indicative of larger SFRs). Moreover, this SFR enhancement is more pronounced at closest pair separations (<30 kpc). Scudder et al. 2012 perform a similar analysis on SDSS pairs and, in addition to SF enhancement, find that SF is most strongly enhanced in major merger systems, hinting that the pair mass ratio is significant in the modification of SF history through galaxy interactions. In a distinct but complementary approach, Owers et al. 2007 find that 2df Galaxy Redshift Survey selected starbursts are more likely to have a neighbour of comparable brightness within 20 kpc, and 30 per cent of starburst galaxies show morphological signatures of interactions and mergers – suggesting that the SF in these systems is induced by a galaxy–galaxy interaction. However, by contrast Li et al. (2008) also find strong enhancement of SF in interactions but suggest that there is little correlation between this enhancement and the relative luminosity of the interacting galaxies (and therefore, pair mass ratio). They do also find that the enhancement of SF is stronger for lower mass systems. By splitting individual interacting galaxies into high ($\langle \log[M^*/M_\odot]\rangle = 10.6$) and low ($\langle \log[M^*/M_\odot]\rangle = 9.72$) stellar mass samples, they find that at a given pair separation, SF is enhanced more strongly in low-mass than high-mass pair galaxies.

Numerical simulations offer further insight into the complexities of these interaction SF processes. Di Matteo et al. 2007 model several hundred galaxy close pair interactions (<20 kpc) for various morphological classes, and find that while SF is primarily enhanced in galaxy interactions, mergers do not always trigger starbursts, and galaxy interactions are not always sufficient to convert high gas masses into new stars. They also highlight that the amount by which SF is enhanced is anticorrelated with pair separation on small scales (i.e. galaxies which have a very close passage produce the lowest bursts of SF), as well as the amplitude of tidal forces (i.e. pairs that undergo less intense tidal forces can preserve higher gas masses for future SF during the merger). These simulations suggest that SF enhancement is not ubiquitous in interactions and that SF is likely to vary as a function of pair separation and pair mass ratio – higher mass ratios will induce more significant tidal effects in the lower mass galaxy in the pair removing the bulk of its gas and as such, starving SF.

Recently we have seen tentative observational evidence in support of these simulation predictions for close pairs. Robotham et al. 2013 studied *L** galaxies in closely interacting pairs taken from the Galaxy And Mass Assembly (GAMA) Galaxy Group Catalogue (G³C), and investigate variations in SF as a function of pair mass ratio. They find that primary (higher mass) pair galaxies have their SF enhanced, but only when the pair mass ratio is close to 1, while the secondary (lower mass) galaxy has its SF suppressed

relative to equivalent stellar mass non-pair galaxies. In addition, De Propris et al. 2014 find that close pair galaxies are consistently redder than a similarly selected comparison sample, and suggest that these systems have been 'harassed' in multiple previous passes prior to the current close interaction. These results give the first tentative observational evidence that SF in interacting systems is more complicated than the traditional evidence would suggest, and highlight that the pair mass ratio may play a vital role in the changes to SF induced by an interaction.

However, questions still remain regarding the details of SF in interacting systems, such as how does SF proceed in interactions as a function of pair separation when considering pair samples split by merger ratio, primary or secondary status and individual galaxy mass? A potentially more significant question is over what time-scales do variations in the SFR in interacting systems become apparent? If we measure SFRs using observational tracers which probe different SF time-scales, will we see differences in observed SFRs? SF enhancement/suppression in interactions is likely to occur on short time-scales, and hence may only be apparent in SFR measures which probe short periods of the galaxy's SF history.

In this paper, we further investigate SF in closely interacting pairs taken from the G³C. We split our sample by merger ratio, primary or secondary status and galaxy mass, and investigate SF characteristics as a function of pair separation. We determine SFRs for each galaxy using multiple nebular emission line and continuum fluxes, which probe the galaxy's SF history over different time-scales, and compare these methods in order to identify short time-scale variations in SF, once again as a function of pair separation. In this manner, we identify factors driving the modification of SFRs in interacting galaxies. In Section 2 we outline the GAMA survey and pair catalogue used in this work, Section 3 discusses the SFR indicators used, in Section 4 we highlight the effects of interactions on SF in galaxies and in Section 6 we summarize our results.

Throughout this paper, we use a standard Λ cold dark matter cosmology with $H_0 = 70$ km s^{-1} Mpc^{-1}, $\Omega_\Lambda = 0.7$ and $\Omega_M = 0.3$.

2 DATA

2.1 GAMA and the pair catalogue

The GAMA survey is a highly complete multi-wavelength data base (Driver et al. 2011) and galaxy redshift (*z*) survey (Baldry et al. 2010; Hopkins et al. 2013; Liske et al., in preparation) covering 280 deg^2 to a main survey limit of $r_{AB} < 19.8$ mag in three equatorial (G09, G12 and G15) and two southern (G02 and G23) regions. The spectroscopic survey was undertaken using the AAOmega fibre-fed spectrograph (Saunders et al. 2004; Sharp et al. 2006) in conjunction with the Two-degree Field (Lewis et al. 2002) positioner on the Anglo-Australian Telescope and obtained redshifts for ∼250 000 targets covering $0 < z \lesssim 0.5$ with a median redshift of $z \sim 0.2$, and highly uniform spatial completeness (Baldry et al. 2010; Robotham et al. 2010; Driver et al. 2011). Full details of the GAMA survey can be found in Driver et al. (2011) and Liske et al. (in preparation). In this work, we utilize the first 5 years of data obtained and frozen for internal team use, referred to as GAMA II.

First, to minimize AGN contamination in our sample, which may potentially bias our SFR estimates, we exclude optically bright AGN using the BPT diagnostic diagram (Baldwin, Phillips & Terlevich 1981). We select sources from the GAMA II spectral line catalogue which have all BPT diagnostic lines detected at S/N > 3, and have emission lines which do not lie at the edge of the spectral range
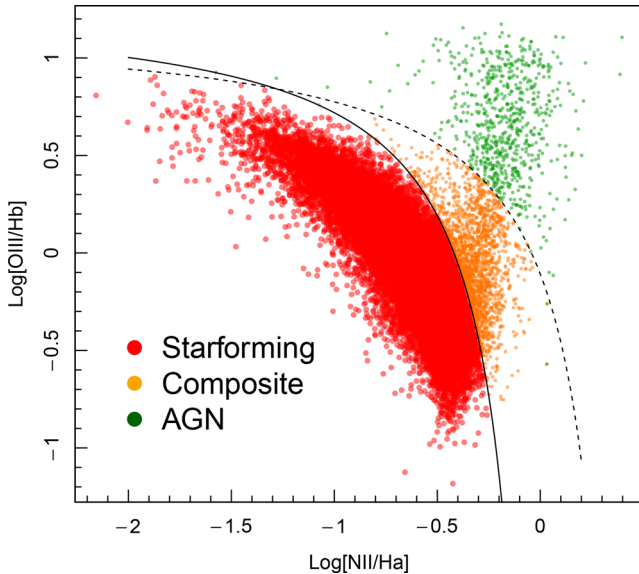
Figure 1. The BPT diagram for all GAMA II sources with all diagnostic emission lines detected at S/N > 3. The AGN dividing line of Kewley et al. (2013) is displayed as the black dashed line, while the composite dividing line of Kauffmann et al. (2003) is shown as the black solid line. Sources which potentially contain AGN are displayed as green or orange.

(and may have poor line measurements). We then apply the BPT AGN+composite source selection line of Kauffmann et al. (2003):

$$\log_{10}([\text{O\,\textsc{iii}}]/\text{H}\beta) > \frac{0.61}{\log_{10}([\text{N\,\textsc{ii}}]/\text{H}\alpha) - 0.05} + 1.3, \qquad (1)$$

to identify galaxies which may have their SFR contaminated by AGN (Fig. 1). Galaxies which meet the BPT AGN selection are coloured green and those which are potentially composite AGN+SF sources are coloured orange. We find a total of 2486 galaxies from the full GAMA II sample which potentially contain an optically bright AGN.

In order to select systems which are undergoing a close interaction, we utilize the GAMA G^{3}C which includes the identification of all galaxy pairs (Robotham et al. 2011, also see Robotham et al. 2012, 2013 and 2014. Briefly, pairs are selected on physical projected separation, $r_{\text{sep-proj}}$ (for the cosmology given in Section 1) and radial velocity separation, $v_{\text{sep-rad}}$. In this paper, we use systems which meet the pair criteria of Robotham et al. 2012, 2013 and 2014:

$$P_{r100v500} = r_{\text{sep-proj}} < 100\,\text{kpc} \wedge v_{\text{sep-rad}} < 500\,\text{km s}^{-1}.$$

This sample consists of a total of 37 679 galaxies in pairs. We further restrict our sample to pairs at $z < 0.3$ in order to minimize the impact of redshift evolution in our galaxies and biases towards the identification of high-mass pairs at the high-redshift end, giving a total of 33 832 pair galaxies. We then match all pair galaxies to the GAMA II panchromatic photometry catalogue (Driver et al., in preparation) and use rest-frame photometry derived from a refactored implementation of the InterRest algorithm (Rudnick et al. 2003; Taylor et al. 2009), coupled with the empirical set of galaxy template spectra of Brown et al. (2014). We exclude any galaxy classed as an AGN using the classifiers described above, leaving 32 468 pair galaxies.

We use the stellar masses derived from the *ugriZJH* photometry for all GAMA II galaxies (Taylor et al. 2011) to assign classes to each individual galaxy. First, we determine whether each galaxy

is the primary or secondary system in the interacting pair (by mass). Secondly, we calculate the pair mass ratio and identify each system as being either part of a major merger (mass ratio < 3:1) or minor merger (mass ratio > 3:1). Note that we also split our minor merger sample further into 3:1<mass ratio<6:1 and mass ratio>6:1 subsamples, but see little difference between each of these populations. As such, we do not discuss them in this work.

A potential caveat to the selection above is that we may be biased towards pair systems where both galaxies are star-forming, specifically at the low-mass and/or high-redshift end – where we are not mass complete. For example, by purely applying a redshift selection, we are more sensitive to higher stellar mass and potentially star-forming galaxies. As such, low-mass systems will only be identified as being in an interaction if both pair galaxies are high mass and/or highly star-forming. Likewise, if we were to only apply a mass selection over the full sample, we do not take into account the broad redshift range of our selection and any evolution of the star-forming properties of galaxies across this extensive look-back time. As such, our pair sample will be biased towards specific galaxy populations and we will dilute any observed trends by not taking into account the global change in SF properties of galaxies with redshift. In order to remove this effect, we compare all of our pair galaxy samples to a mass- and redshift-matched control sample. The control sample contains the same mass bias and redshift evolution as the pair sample, and as such removes any dependence on this effect (GAMA is essentially 100 per cent complete in the *r* band; thus, sources will also not drop out of our pair selection preferentially to our control sample due to the effect of the interaction on SF – where the *r* band will not be strongly affected). As such, we can directly compare the effects of an interaction to non-interacting galaxies at the same stellar mass and redshift. Our control sample is defined further in Section 4.2. In this paper, we only display our results in comparison to this control sample, and as such are not biased by our mass incompleteness.

We note that in defining our control sample based on stellar mass and redshift, we are not taking into account the different galaxy clustering statistics of passive and active systems. Passive galaxies are more strongly clustered (e.g. Zehavi et al. 2011), and as such more likely to be in pairs (see Lin et al. 2008; de Ravel et al. 2009, for the fraction of quiescent galaxies in major mergers at $z \sim 0$). This could potentially bias our control sample towards a higher fraction of actively star-forming systems. However, we do not wish to perform any sample selection based on SF diagnostics, as the increased fraction of passive systems in pair galaxies may in fact be caused by the galaxy interactions – the very effect we wish to measure here. As we will see, the majority of subsamples in our analysis show enhanced SF in close pairs, a result that would only be reduced by the potential biases discussed above. In addition, we see distinct differences between the primary and secondary galaxies of minor mergers in our sample. Any bias produced by different clustering statistics would affect both populations in the same manner. Hence, such a bias is unlikely to be driving this result.

In all of the subsequent analysis in this paper, we consider each pair galaxy member individually, but split our samples into primary and secondary galaxies, and major and minor mergers based on the classification within their pair system. We also further split our samples by the stellar mass of each individual galaxy as noted above. For reference, Table 1 shows the number of galaxies in each mass bin as a function of primary or secondary status and major or minor merger classification.

Table 1. Number of pair sources (each pair galaxy is treated individually) in each mass bin as a function of primary or secondary system status and major or minor merger classification.

Mass range ($\log_{10}[M_\odot]$)	Total	Primary	Secondary	Major	Minor
9.5–10.0	4606	1407	3199	2088	2517
10.0–10.5	8795	3958	4837	5121	3670
10.5–11.0	10 910	7282	3628	6870	4040
All	24 311	12 647	11 664	14 079	10 227
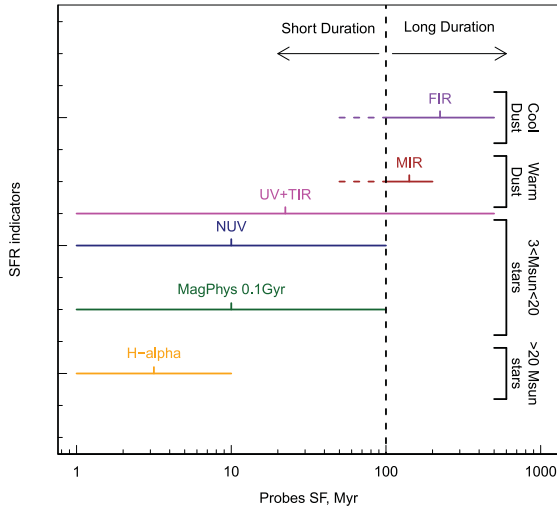
Figure 2. SF time-scale probed by each SFR indicator used in this work, for normal disc galaxies. Sources of the emission are noted on the right-hand side of the figure. We split our measures into short (<100 Myr) and long (>100 Myr) duration. See the text for details of each SFR indicator.

3 SF MEASURES OVER DIFFERENT TIME-SCALES

In this paper, we consider SFRs determined via different observables in order to probe SF on different time-scales and equate them to recent variations in the galaxy's instantaneous SFR. Fig. 2 shows a cartoon pictorial representation of the time-scales over which each SFR indicator (described in more detail below) probes in normal disc galaxies and the source of the emission in each case. This figure is only intended to highlight the key differences in time-scales over which each indicator probes, as the complex physics of each process is likely to place large variation on the true time-scale of the emission arising from each source. As such, we do not constrain our SFR indicators further than splitting them into long-duration – probing time-scales >100 Myr, far-infrared (FIR), UV+total infrared (UV+TIR) and mid-infrared (MIR) – and short-duration SFR indicators, probing only <100 Myr, FUV, near-ultraviolet (NUV), MAGPHYS (0.1 Gyr) and Hα. See Gilbank et al. 2010 for a comparison of different SFR indicators in the SDSS stripe 82 and details of each SFR indicator used in this work below.

3.1 Long-duration MIR/FIR continuum SFRs

Infrared (IR) emission at 1–1000 μm arising from 'normal' star-forming galaxies is produced from three sources: photospheres and circumstellar envelopes of old stars undergoing mass-loss (e.g. Melbourne et al. 2012), interstellar gas and dust heated by either bright

OB stars in star-forming regions (warm dust) or the general stellar radiation field throughout the interstellar medium (cool dust – 'cirrus') – for example see the review by Sauvage, Tuffs & Popescu (2005), Popescu et al. 2000 or more recently Xilouris et al. 2012 and references therein. Stellar sources of IR emission dominate at short wavelengths <3 μm and interstellar gas emission makes up just a few per cent of the TIR output of galaxies. At 3-100 μm, the bulk of the emission arises from warm dust locally heated by UV emission from young stars in star-forming regions, with cirrus emission dominating at >60 μm. As such, probing IR flux from star-forming galaxies in the 3-100 μm range gives a reliable estimate for the ongoing SF (e.g. Calzetti et al. 2007, the amount of flux emitted in the IR is directly related to the UV emission from newly formed stars). However, IR emission from dust requires significantly long time-scales to become apparent and subsides slowly when SF is suppressed (see Kennicutt 1998). As such, SFRs derived from the IR continuum probe SF over large time-scales, giving an estimate of a galaxy's SF history on time-scales of $\gtrsim 100$ Myr.

In this paper, we consider two IR continuum measures of SFR. First, we determine the FIR SFRs derived from the 100 μm flux provided for all GAMA sources as part of the *Herschel* Astrophysical Terahertz Large Area Survey (H-ATLAS; Eales et al. 2010) and outlined in the GAMA II panchromatic data release (Driver et al., in preparation). The 100 μm data come from the H-ATLAS Phase 1 Data Release (Valiante et al., in preparation), which provides Photoconductor Array Camera and Spectrometer (PACS) maps at 100 and 160 μm reduced using SCANAMORPHOS. The GAMA II photometry in the *Herschel* maps exploits an algorithm developed by Bourne et al. 2012 to optimally capture extended flux while accounting for blending in the low-resolution images. This algorithm consists of convolving the 100 μm map with a kernel given by the GAMA *r*-band-defined aperture smoothed with the 9 arcsec (full width at half-maximum, FWHM) point spread function (PSF) of the PACS 100 μm band. These smoothed apertures are created for all GAMA galaxies, and any that overlap in the map are down-weighted so that the 100 μm flux in such pixels is shared between the overlapping apertures. Fluxes in all other H-ATLAS bands are used for the UV+TIR and MAGPHYS SFRs (see below) and are produced in a similar manner, but using different PSFs – which are specific to the band in question. For more details, see Bourne et al. 2012 and Driver et al. (in preparation). We convert 100 μm fluxes to SFRs using the tight correlation derived in Davies et al. 2014 for Virgo cluster galaxies:

$$\log_{10} \text{SFR}_{\text{FIR}}(M_\odot \, \text{yr}^{-1}) = 0.73 \log_{10} L_{100\,\mu\text{m}}(\text{W Hz}^{-1}) - 17.1. \quad (2)$$

Secondly, we derive MIR SFRs using the *Wide-field Infrared Explorer* (*WISE*) data from the matched GAMA-*WISE* catalogue outlined in Cluver et al. 2014. We use *WISE* 22 μm (*W*4) band fluxes, which are not strongly affected by polycyclic aromatic hydrocarbon emission, and the best-fitting SFR correlation obtained in Cluver et al. 2014:

$$\log_{10} \text{SFR}_{\text{MIR}}(M_\odot \, \text{yr}^{-1}) = 0.84 \log_{10} \nu L_{22\,\mu\text{m}}(L_\odot) - 7.3. \quad (3)$$

We note that the correlations derived in Cluver et al. 2014 compare *WISE* fluxes with Hα-derived SFRs, and as such may be biased towards emission line-derived SFRs. However, we rescale all SFRs derived in the paper to have the same slope and normalization as the SFR$_{\text{FIR}}$ in order to compare each measure directly (see below).

3.2 Short-duration attenuation-corrected UV continuum and MAGPHYS SFRs

In contrast to the FIR and MIR, UV continuum-derived SFRs probe a shorter time-scale than those in the IR ($\lesssim 100$ Myr). UV continuum arises from hot, massive ($M_* > 3\,\mathrm{M}_\odot$) O and B stars, and as such is a good tracer of more recent SF in galaxies (e.g. Kennicutt & Evans 2012), with luminosity-weighted mean ages for a constant SFR predicted to be ~ 28 Myr for the *GALEX* FUV band and ~ 80 Myr for *GALEX* NUV (Grootes et al., in preparation).

Hence, by comparing IR continuum and UV continuum SFRs, we may be able to disentangle recent SF changes in a system – potentially due to interactions.

However, direct estimates of the SFR from UV continuum luminosities are problematic as the UV emission arising from a galaxy is extremely sensitive to dust attenuation (e.g. Wang & Heckman 1996). Previous studies have attempted to overcome this issue through estimating attenuation-corrected SFRs by applying attenuation estimates based on the UV spectral slope (β) and luminosity corrections, such as those derived by Meurer, Heckman & Calzetti (1999) – e.g. Wijesinghe et al. 2011. Such corrections apply general scaling to all galaxies and may not be appropriate for specific galaxy classes (e.g. Wilkins et al. 2012), severely biasing any results derived by such an analysis.

Here we take a different approach and use the full spectral energy distribution (SED) MAGPHYS (da Cunha, Charlot & Elbaz 2008) fits to the GAMA II galaxies (Driver et al., in preparation). In this upcoming work, Driver et al. obtain the best SED fit to the full 21-band photometric data available to all GAMA II sources, simultaneously fitting the UV through FIR flux and obtaining the best-fitting unattenuated model spectrum. For our attenuation-corrected UV luminosities, we use the unattenuated UV emission from the best-fitting MAGPHYS model template convolved with the *GALEX* FUV/NUV filter curves. In this manner, we use each galaxy's full SED to estimate the attenuation correction to be applied to the UV luminosity for each individual galaxy instead of applying a general β correction. We convert UV luminosity to SFR using the calibrations given in Wijesinghe et al. 2011:

$$\mathrm{SFR_{NUV}}(\mathrm{M}_\odot\,\mathrm{yr}^{-1}) = \frac{L_{\mathrm{NUV}}(\mathrm{W\,Hz}^{-1})}{1.56 \times 10^{21}}, \qquad (4)$$

$$\mathrm{SFR_{FUV}}(\mathrm{M}_\odot\,\mathrm{yr}^{-1}) = \frac{L_{\mathrm{FUV}}(\mathrm{W\,Hz}^{-1})}{1.64 \times 10^{21}}. \qquad (5)$$

The MAGPHYS code also provides an estimate of the galaxy SFR averaged over the last 100 Myr using a best-fitting model for both the FIR and UV emission for a combined estimate of both obscured and unobscured SF (hereafter $\mathrm{SFR_{0.1\,Gyr}}$). Hence, this provides an additional short time-scale SFR estimate with which we compare our long-duration $\mathrm{SFR_{FIR}}$.

3.3 Long-duration UV continuum + TIR luminosity SFR

We also use the combination of UV and TIR luminosities as an SFR proxy broadly probing the last ~ 300 Myr of the galaxies SF history. As discussed above, UV emission arises directly from star-forming regions and probes SF on short time-scales, while some fraction of this emission is absorbed and reprocessed by dust, being re-emitted in the FIR on longer time-scales. As such, using a SFR indicator which probes both the UV and FIR emission gives a relatively stable, but broad time-scale, measure of SF in our sample galaxies. We therefore sum both UV and TIR luminosities to obtain a total SFR estimate, based on the bolometric luminosity of OB stars.

We use the method outlined in many high-redshift studies (e.g. Bell et al. 2005; Papovich et al. 2007; Barro et al. 2011) of

$$\mathrm{SFR_{UV+TIR}}(\mathrm{M}_\odot\,\mathrm{yr}^{-1}) = 1.09 \times 10^{-10}[L_{\mathrm{IR}} + 2.2L_{\mathrm{UV}}](\mathrm{L}_\odot). \qquad (6)$$

This prescription is the Bell et al. 2005 recalibration of the relation from Kennicutt 1998, scaled for a Chabrier 2003 stellar initial mass function (IMF). Here, L_{IR} is the total IR luminosity, integrated between 8 and 1000 μm. These values have been estimated by fitting the Chary & Elbaz 2001 galaxy templates to the *WISE* and *Herschel* photometric points. The bolometric UV luminosity between 1216 and 3000 Å, L_{UV}, is estimated as $1.5\nu f_{\nu,\,2800}$, where $f_{\nu,\,2800}$ is the rest-frame luminosity at 2800 Å. For further details of this process, see Taylor et al. (in preparation).

3.4 Short-duration nebular Hα SFRs

Hα photons arise from gas ionized by the stellar radiation field, and only stars with ages <20 Myr can contribute significantly to this ionizing flux. Thus, Hα provides a direct measure of the current SFR in galaxies (<10–20 Myr) which is largely independent of SF history (e.g. see Kennicutt 1998).

For $\mathrm{SFR_{H\alpha}}$ we use emission line data from the GAMA II spectroscopic campaign (Owers et al., in preparation), where aperture-, obscuration- and stellar absorption-corrected Hα luminosities are given by

$$L_{\mathrm{H\alpha}} = (\mathrm{EW_{H\alpha}} + \mathrm{EW_c}) \times 10^{-0.4(M_r - 34.1)}$$

$$\times\, \frac{3 \times 10^{18}}{(6564.1(1+z)^2)} \left(\frac{F_{\mathrm{H\alpha}}/F_{\mathrm{H\beta}}}{2.86} \right)^{2.36}, \qquad (7)$$

and $\mathrm{EW_{H\alpha}}$ denotes the Hα equivalent width, $\mathrm{EW_c}$ is the equivalent width correction for stellar absorption (2.5 Å for GAMA; Hopkins et al. 2013), M_r is the galaxy r-band magnitude and $F_{\mathrm{H\alpha}}/F_{\mathrm{H\beta}}$ is the Balmer decrement (see Gunawardhana et al. 2011, for further details). Using this, $\mathrm{SFR_{H\alpha}}$ can be determined from Kennicutt 1998, assuming a Salpeter IMF:

$$\mathrm{SFR_{H\alpha}}(\mathrm{M}_\odot\,\mathrm{yr}^{-1}) = \frac{L_{\mathrm{H\alpha}}(\mathrm{W\,Hz}^{-1})}{1.27 \times 10^{34}}. \qquad (8)$$

One caveat to using Hα SFRs is that the aperture-based spectroscopy only probes the central regions of nearby galaxies. However, in this paper we only investigate SFRs in comparison to a control sample of galaxies matched on mass and redshift (see below), and as such both our pair and control sample should suffer the same aperture bias.

We note that the GAMA stellar masses, UV+TIR and MAGPHYS-based SFRs are calculated assuming a Chabrier IMF, while our Hα, MIR and FIR SFRs are calculated using a Salpeter IMF, as such we scale all Salpeter IMF SFRs by a factor of 1.5 to account for this discrepancy (Davé 2008; Driver et al. 2013). In addition, all results in this work are displayed relative to a control sample with SFRs derived in an identical manner. As such, differences between IMF assumptions in different indicators will not affect our results.

3.5 Calibrating continuum SFRs

As noted above, we recalibrate all continuum SFR measures to have the same slope and normalization as $\mathrm{SFR_{FIR}}$. We apply this correction as all SFR indicators are derived using vastly different calibrations and different samples. If SFR indicators consistently derived SFRs in the same manner, we would find a similar slope and normalization when comparing indicators. In Fig. 3, we display
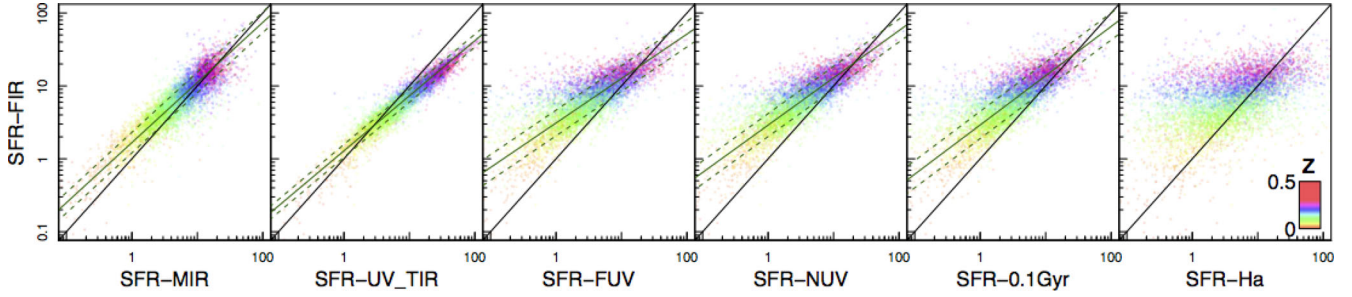
Figure 3. Comparisons between various SFR measures used in this work. The 1:1 relation is shown by the solid black line. Points are colour coded by source redshift, z. HYPERFIT best-fitting lines to each correlation are displayed as the green lines with $\pm 1\sigma$ errors on the normalization. These fits are used to scale each distribution to the same slope and normalization using equation (9). Note that we do not scale $SFR_{H\alpha}$ as the correlation between SFRs is poor.

our SFR indicators in comparison to SFR_{FIR} for all sources detected at $S/N > 2$ in both the *Herschel* 100 µm and *WISE* $W4$ observations (the limiting bands in our selection). Clearly, not all indicators show the same slope and normalization. These offsets are likely to be produced by the SF calibration, not the true galaxy population. As such, we fit the slope and normalization of each distribution using the [R] multi-dimensional Markov Chain Monte Carlo fitting procedure, HYPERFIT (Robotham & Obreschkow, in preparation) and recalibrate each SFR measure using the best-fitting parameter as follows:

$$\log_{10} SFR_{cal} = a \times \log_{10} SFR_{orig} + b, \tag{9}$$

where

SFR_{MIR}, $a = 0.824 \wedge b = 0.223$

SFR_{UV+TIR}, $a = 0.755 \wedge b = 0.110$

SFR_{FUV}, $a = 0.610 \wedge b = 0.491$

SFR_{NUV}, $a = 0.649 \wedge b = 0.462$

$SFR_{0.1\,Gyr}$, $a = 0.595 \wedge b = 0.562$

$SFR_{H\alpha}$, $a = 1 \wedge b = 0$.

Note that we do not apply a correction to the Hα emission line-derived SFR as there is large scatter in the distribution but the locus follows a 1:1 correlation. In fact, this scatter could be due to the very time-scale variations we hope to identify in this work – short time-scale variations will be most apparent through a comparison of Hα- and FIR-derived SFRs. We explore this further in Section 5.1. While we apply these calibrations to form the main comparison in this work, we note that our conclusions hold true if no correction is applied. A comparison of SFR indicators for the full GAMA II sample will be the subject of an upcoming paper (Davies et al., in preparation).

One potential caveat to these scalings is that they are defined only for FIR detected sources, and may not be applicable to the general galaxy population. To highlight the fact that it is unlikely to cause significant bias in our results and that these scalings are appropriate, Fig. 4 shows the main sequence of star-forming galaxies for a completely independent SFR indicator not used in this work. Here we use the extinction-corrected NUV SFR (using the direct NUV fluxes and UV spectral slope extinction correction, unlike the MAGPHYS NUV fits used elsewhere in this work), which does not use any information from the FIR [this SFR indicator will be defined
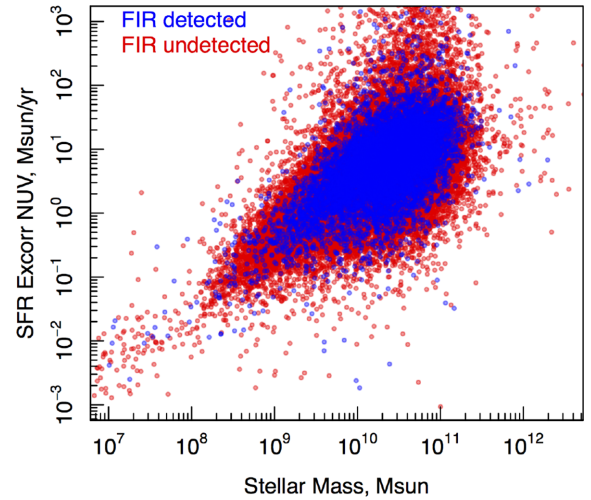
Figure 4. The main sequence of star-forming galaxies for extinction-corrected NUV SFRs (see the text for details). FIR detected sources are shown as blue points, while FIR undetected sources are shown as red points. Both populations are consistent, and as such correlations derived for the FIR detected sources are applicable to the full sample.

further in Davies et al. (in preparation)]. For all GAMA II galaxies in our redshift- and mass-limited sample, we display sources with FIR detections ($>2\sigma$) as blue points, and those without FIR detections as red points. Clearly, the main sequence is consistent between FIR detected and undetected sources, suggesting that any correlation derived from the FIR detected sample is applicable to all galaxies.

In the following analysis, unless otherwise stated, we use specific SFRs (sSFRs) calculated by dividing all measured SFRs by stellar mass. This removes any mass dependence on observed SFR correlations.

4 SF IN PAIR GALAXIES AS A FUNCTION OF PAIR SEPARATION

In attempting to pin down the effect of close interactions on galaxy SFRs, we have two measurements which can both be considered as a proxy for the stage of interaction which we are witnessing: (i) pair separation and (ii) SFRs on different time-scales. In the former, to first order, we can equate the pair separation to stage of the interaction – in that distant pairs are more likely to be at an early stage and close pairs at a later stage of the interaction (we will discuss the caveats to this assumption in Section 6). Therefore, we may expect galaxies at large pair separations to display SFRs which

are not strongly affected by the interaction and close pairs to show the strongest effects. In the latter, we are directly measuring SFRs at different stages of the interaction. As such, we may expect long-duration SFR indicators to probe an epoch prior to the modification of SF, while short-duration indicators should once again show the strongest affect.

In the following three subsections, we separate out the variations with pair separation alone, considering each SFR indicator independently, and do not discuss the use of multiple indicators to highlight short-duration time-scale changes. However, when reading the following analysis we encourage the reader to keep in mind that pair separation is a proxy for time-scale within the interaction. The following sections discuss the fine details of SFR variation in pairs and we direct the casual reader to Section 4.2.1 for a summary of the key results found in the following section and Section 6 for a full summary of all of our results.

4.1 Comparisons between pair samples in Robotham et al. (2014)

Initially, we compare different SFR indicators for our pair sample as a whole (not split by mass, pair mass ratio, etc.) in order to highlight discrepancies in the results derived from previous studies probing SF in interacting systems. We split our pair systems based on the three pair selection criteria outlined in Robotham et al. (2014):

$$P_{r20v500} = r_{sep} < 20\,h^{-1}\,\mathrm{kpc} \wedge v_{sep} < 500\,\mathrm{km\,s^{-1}},$$

$$P_{r50v500} = r_{sep} < 50\,h^{-1}\,\mathrm{kpc} \wedge v_{sep} < 500\,\mathrm{km\,s^{-1}},$$

$$P_{r100v1000} = r_{sep} < 100\,h^{-1}\,\mathrm{kpc} \wedge v_{sep} < 1000\,\mathrm{km\,s^{-1}}, \quad (10)$$

with each sample excluding sources in the inner contained samples (i.e. galaxies in the $P_{r20v500}$ sample are not contained in the $P_{r50v500}$ or $P_{r100v1000}$ sample). Hereafter we define these samples as close, intermediate and far pairs, respectively. We calculate the median $\log_{10}[\mathrm{sSFR}]$ for each indicator and normalize to the value for far pairs – to highlight variations in sSFR between closely interacting and distant systems. Fig. 5 shows the difference between pair samples for each SFR indicator; points are offset for each pair sample in the x-direction for clarity. Error bars display the standard error on the median for each sample, where for many points this is smaller than the plotted symbol. In normalizing to the far-pair systems, positive values in Fig. 5 indicate that SF is enhanced relative to the far-pair sample, while negative values display that it has been suppressed. We find that when measuring SFRs in the FIR, MIR and using UV+TIR SFRs, we would see either no change or in fact suppression of sSFR with pair separation, while for other SFR indicators (FUV, NUV, 0.1 Gyr and Hα) we would see net enhancement of SF. The most significant variation is seen in the $\mathrm{SFR}_{H\alpha}$, where sSFRs appear strongly enhanced by an interaction for both the intermediate- and close-pair samples. This echoes the findings of Patton et al. (2013) and others who find strong enhancements in emission line-derived SFRs.

While the results discussed above are seemingly in conflict (or at least highlight that care must be taken when comparing different SFR indicators), they do not consider the vastly different properties of both the individual galaxies and the merger as a whole. In the following subsections, we shall investigate this further by splitting our samples by stellar mass, primary (higher mass)/secondary (lower mass) status and pair mass ratio, and considering variations in SF as a function of pair separation directly (rather than binning into close, intermediate and far pairs). For completeness, in Appendix A
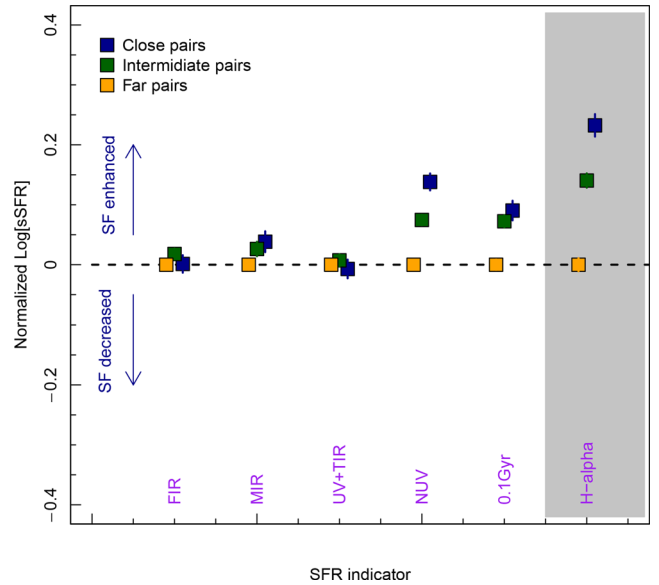
Figure 5. Comparison of SFR indicators for pair galaxy samples discussed in Robotham et al. (2014). Points display the median sSFR for each indicator, while errors show the standard error on the median. All points are normalized to the far pairs' value to highlight differences between far, likely non-interacting, and close, interacting, pairs. SFR indicators are ordered from long to short duration (left to right). SF appears either constant or increased for close pairs in comparison to far pairs depending on the SFR indicator used.

we display the samples defined in Robotham et al. (2014) but split further into major/minor mergers and primary/secondary status.

4.2 Independent measures of SF as a function of pair separation, pair mass ratio and pair status

In this section, we split our pair galaxy sample into stellar mass bins of $\Delta\log_{10}[M^*] = 0.5$ from $10^{9.5}$ to $10^{11.0}$ M$_\odot$. We do not include galaxies outside of this mass range, where sample sizes are too low to apply the analysis discussed in this work. We are currently investigating SF in $M^* < 10^{9.5}$ M$_\odot$ pair galaxies using a different, but complementary, approach – this will be the subject a future work (Davies et al., in preparation).

We then bin on $\Delta r_{sep} = 10$ kpc h^{-1} scales (i.e. ignoring line-of-sight separations which provide little information about the initial pair selections).

As discussed previously, we calculate the excess SF for each indicator in comparison to a mass- and redshift-matched control sample. In order to define this control sample, for each pair galaxy in our sample we select three corresponding non-pair GAMA galaxies, which are the closest match in stellar mass and redshift parameter space (determined by the closest match in 2D space in terms of 3σ clipped standard deviation in each parameter). We do this in each stellar mass, pair mass ratio, primary/secondary status and pair separation bin, such that each date point is scaled appropriately for its matched control sample.

For each sample, mass range and radial separation bin, we then calculate the 3σ clipped mean sSFR for both pair and control galaxies. We define the $\mathrm{SFR_{excess}}$ as the ratio of the mean $\log[\mathrm{sSFR}]$ in pair galaxies, divided by the mean $\log[\mathrm{sSFR}]$ of non-pair galaxies, as follows:

$$\log_{10}[\mathrm{SFR_{ex}}(M^*, r_{sep})] = \frac{\mu(\log_{10}[\mathrm{sSFR_{pairs}}(M^*, r_{sep})])}{\mu(\log_{10}[\mathrm{sSFR_{control}}(M^*, r_{sep})])}. \quad (11)$$

Note that the results discussed in this paper are not sensitive to the choice of mean/median and all trends are observable when using median distributions over 3σ clipped means. We do not show the median distributions here for sake of clarity. Table 2 displays the number of sources used in each sample.

The left columns of Figs 6–11 display SFR$_{\text{excess}}$ for our full sample of pair galaxies as a function of pair separation split by stellar mass and into primary and secondary galaxy within the pair (green and orange lines, respectively). The coloured polygons show the standard error on the mean for the pairs and non-pairs summed in quadrature at each radial distance. In the middle and right columns of these figures, we split our samples further into major and minor mergers, respectively.

Table 2. Number of pair galaxies used in our analysis for each SFR indicator.

Indicator	Number of pair galaxies
FIR	12 168
MIR	4520
UV+TIR	10 678
FUV	24 285
NUV	24 285
0.1 Gyr	24 285
Hα	20 170
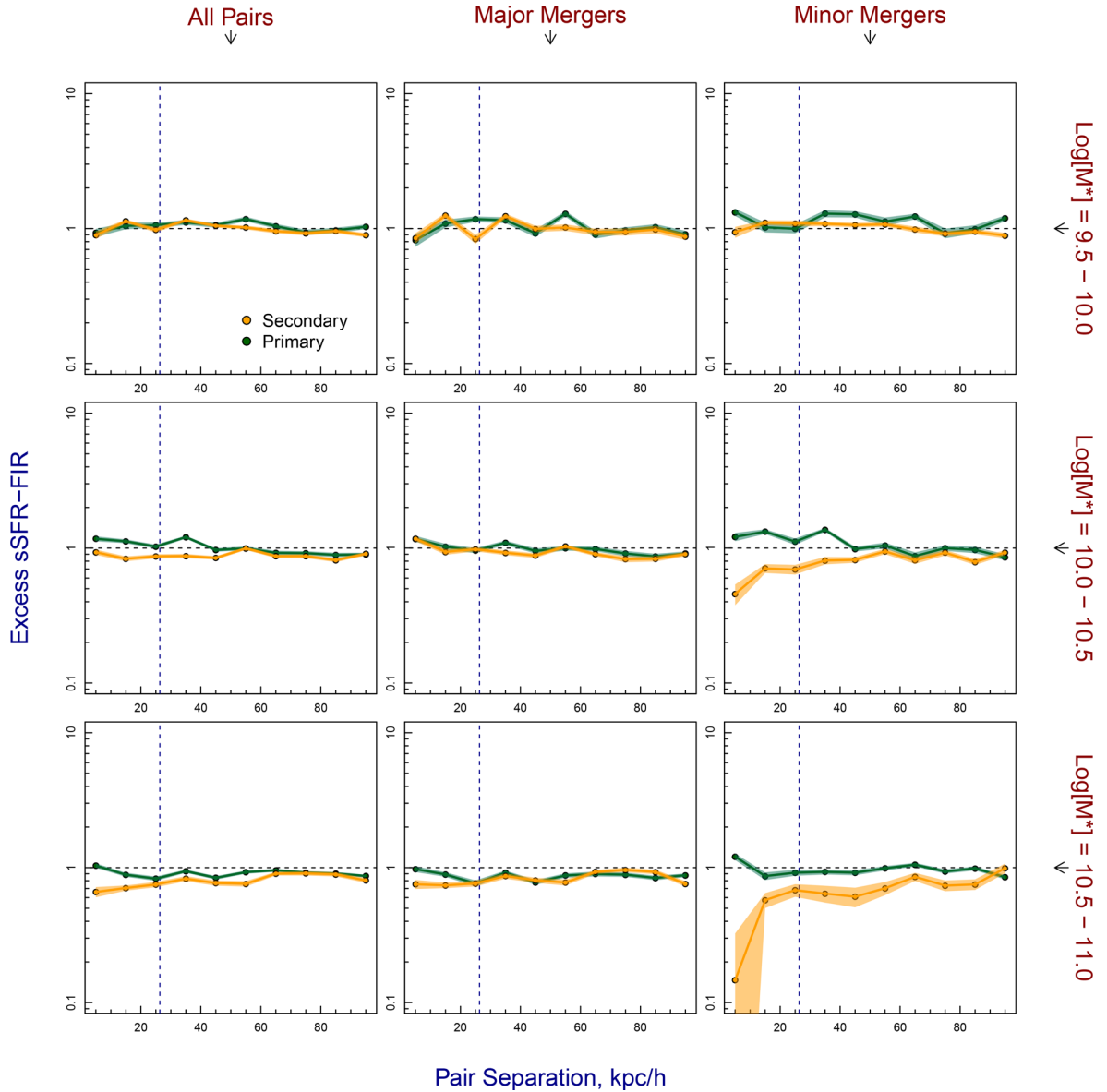
Figure 6. The 3σ clipped mean excess $\log_{10}[\text{sSFR}_{\text{FIR}}]$ for pair galaxies as a function of pair separation binned on $\Delta r_{\text{sep}} = 10\,\text{kpc}\,h^{-1}$ scales. Coloured polygons show the standard error on the mean at each separation. We split out pair samples by stellar mass (rows), into major and minor mergers (separated at 3:1 pair mass ratio – columns) and by primary or secondary status within the pair (green and orange lines, respectively). Blue dashed vertical line shows the FWHM of the PSF of the PACS 100 μm instrument at the median redshift of our pair samples.
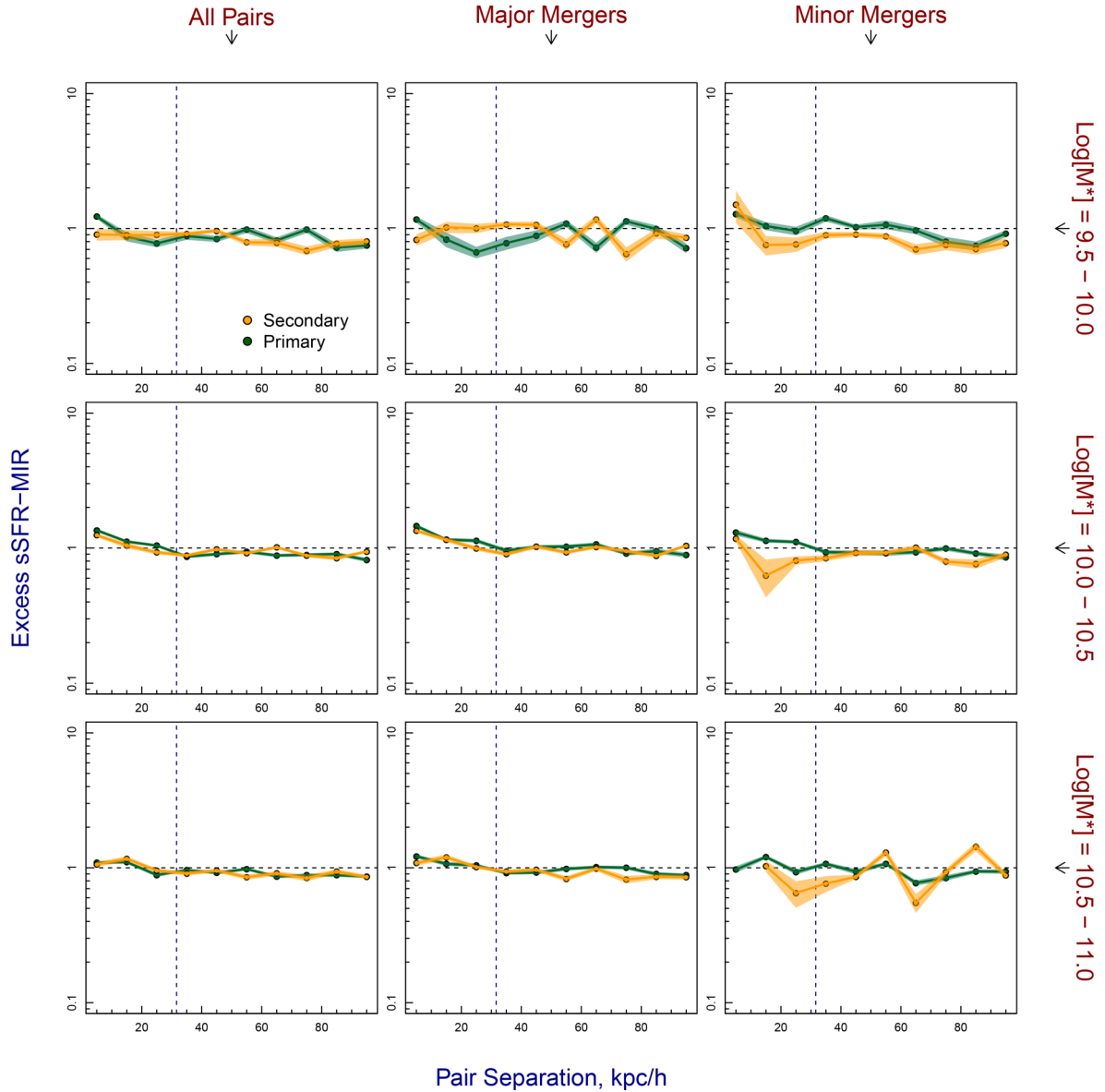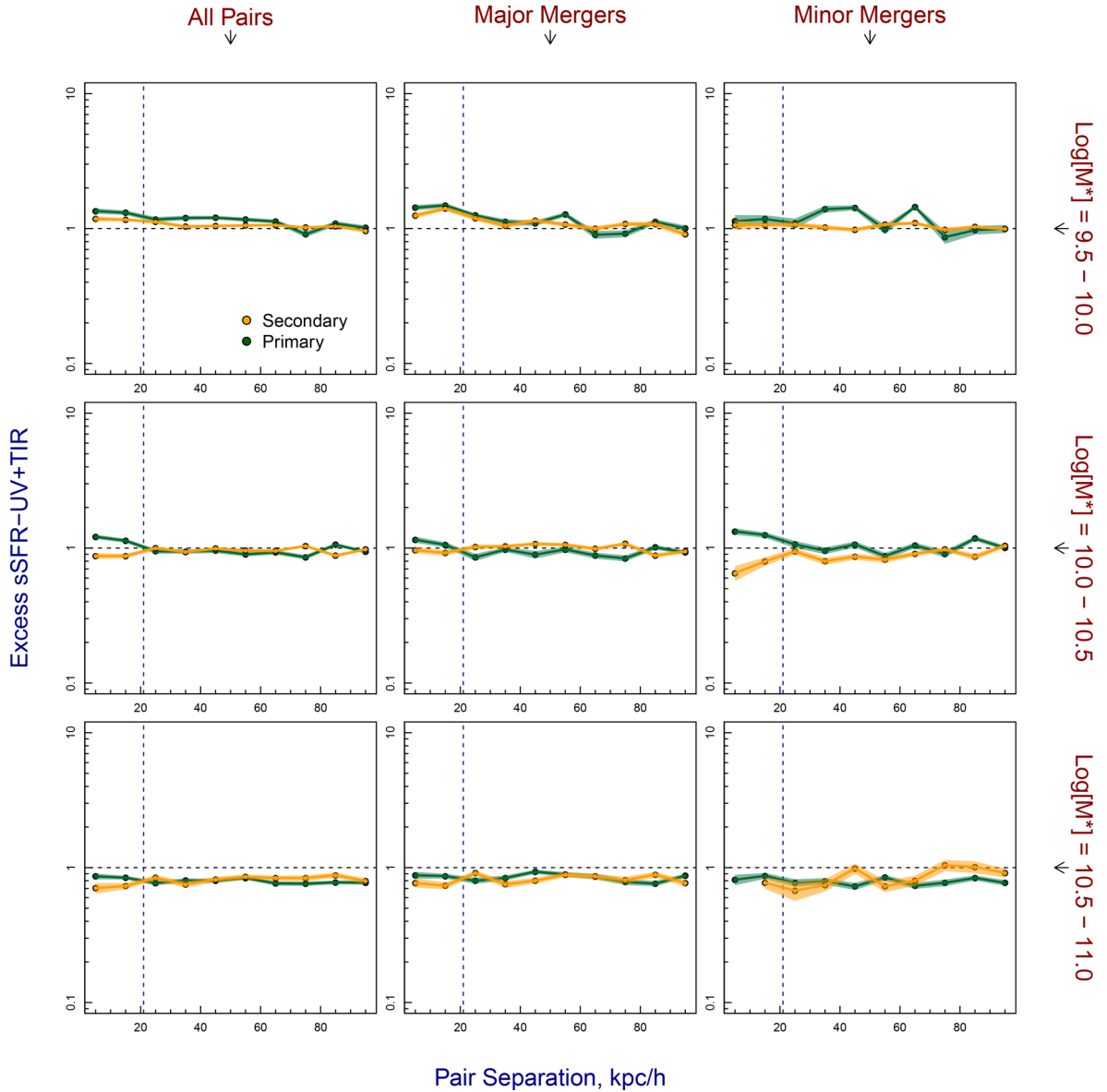
Figure 7. Same as Fig. 6 but for sSFR$_{MIR}$. Green dashed vertical line shows the FWHM of the PSF of *W*4 at the median redshift of our pair samples.

A potential pitfall of this analysis is that poor resolution of continuum observations used in this work means that in many cases close systems share the same resolution element. While attempts have been made to deblend fluxes into individual sources, this may lead to systematic errors in our result. For instance, the secondary galaxy in a pair may have its emission systematically boosted/suppressed via deblending with the primary galaxy and vice versa. In the following figures, we display the physical size of the PSF FWHM of the primary instrument used in calculating the SFR, scaled to the median redshift of our pair sample, as a dashed blue vertical line. As such, sources within this line may have uncertainties on their SFRs which arise from source confusion. However, we note that if real, such uncertainties in this region should be mirrored between primary and secondary populations, i.e. if secondary galaxies systematically have their fluxes underestimated at close pair separations, then primary galaxies should systematically have their fluxes enhanced, as the total flux must be distributed between the

two sources via deblending. This effect is also likely to be minimal in the MAGPHYS results which use the full SED to estimate SFRs. We also note that this effect will not be apparent in the Hα measurements, where the fibre aperture size is much smaller than the physical separation between galaxies. In Section 5.2, we compare the slopes of these distributions. However, we note here that we consider slopes for both the full range of pair separations and only at separations larger than the blue line (and so not affected by source confusion) and the results are consistent, albeit at lower significance.

Below we highlight key observables from Figs 6–11; these will be discussed further in the following sections.

(i) SFR$_{FIR}$ (Fig. 6) – First considering our full sample (left column), we find no strong enhancement or suppression of SFR$_{FIR}$ as a function of pair separation – with both primary and secondary pair galaxies showing no real excess/deficit in comparison to the

Figure 8. Same as Fig. 6 but for sSFR$_{\rm UV+TIR}$. Green dashed vertical line shows the FWHM of the PSF of *GALEX* NUV at the median redshift of our pair samples.

control sample at all pair separations. This is consistent with the results seen in Fig. 5, that there is no significant difference in FIR measured sSFR when considering close, intermediate and far pairs. Splitting this sample into major and minor mergers, we find that the major merger systems (middle column) are almost identical to the full pair sample and also show no excess/deficit in SF.

However, in minor merger systems we see some differences between primary and secondary galaxies. Primary galaxies show marginal enhancement of SF as a function of decreasing pair separation (especially in the $10.0 < \log_{10}[M^*] < 10.5$ range – middle panel of the right column), while secondary galaxies show a deficit in SF in comparison to the control sample. This suppression also appears stronger with increasing stellar mass (from top to bottom of the right column). We also note that, while this suppression is most apparent at very close pair separations, the trend of increasing deficit in SF as a function of pair separation begins outside of the PACS 100 µm

PSF (blue vertical dashed line) and as such is not likely to be driven by deblending confusion.

(ii) SFR$_{\rm MIR}$ (Fig. 7) – For all samples using our MIR SFR indicator, we see marginal enhancement of SF as a function of decreasing pair separation (all samples have a weak slope which increases to small pair separations). We see little difference between primary and secondary galaxies in all samples.

(iii) SFR$_{\rm UV+TIR}$ (Fig. 8) – For our UV+TIR SFR indicator, we find no strong enhancement/suppression of SF with decreasing pair separation. We do see some enhancement in SF for major mergers in our lowest mass bin (top panel of the middle column), and a minor difference between the primary and secondary galaxies in minor mergers at $10.0 < \log_{10}[M^*] < 10.5$ (middle panel of right column).

(iv) SFR$_{\rm NUV}$ (Fig. 9) – For the first of our short-duration SFR indicators (<100 Myr), we start to see strong trends in our samples
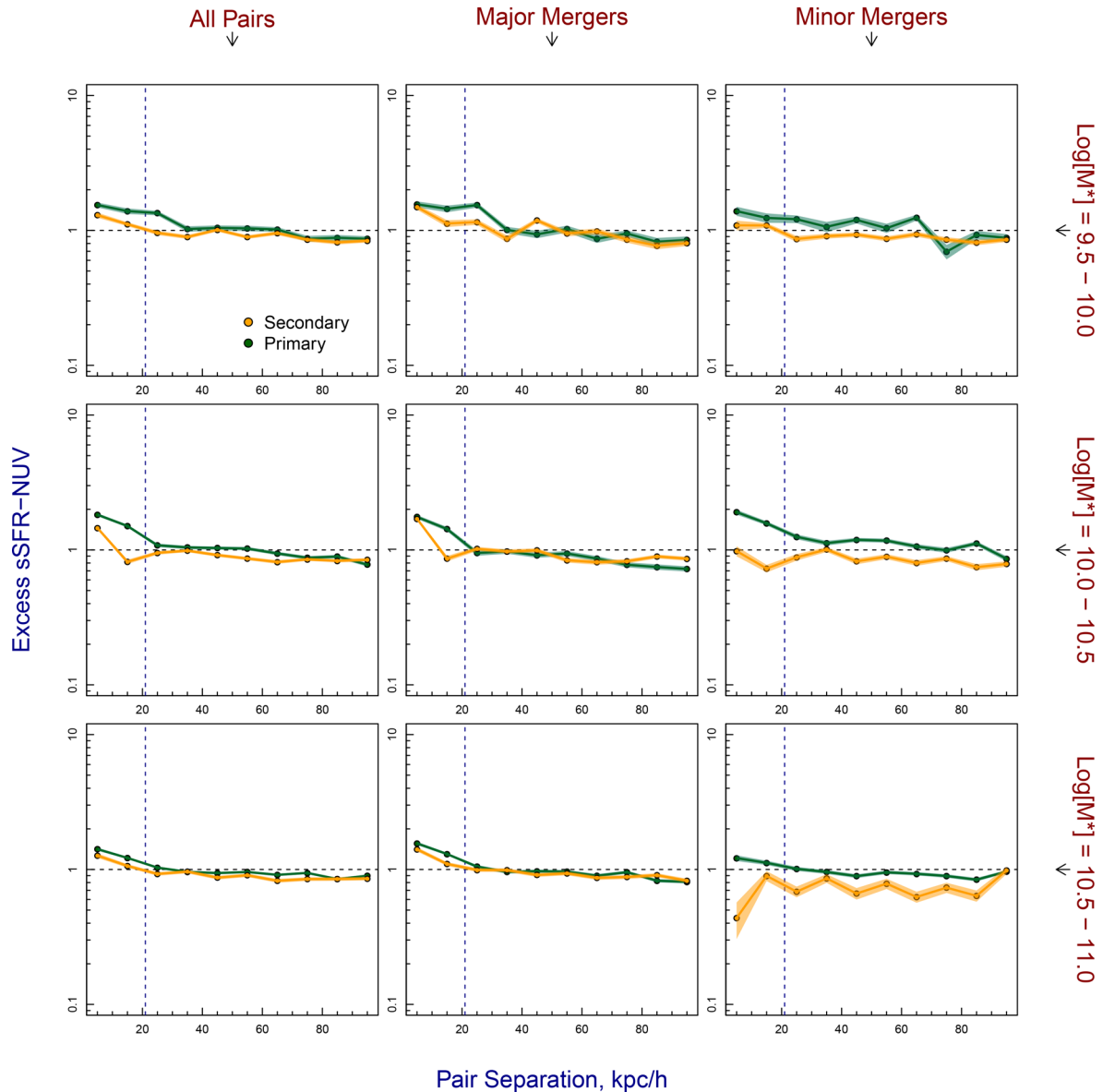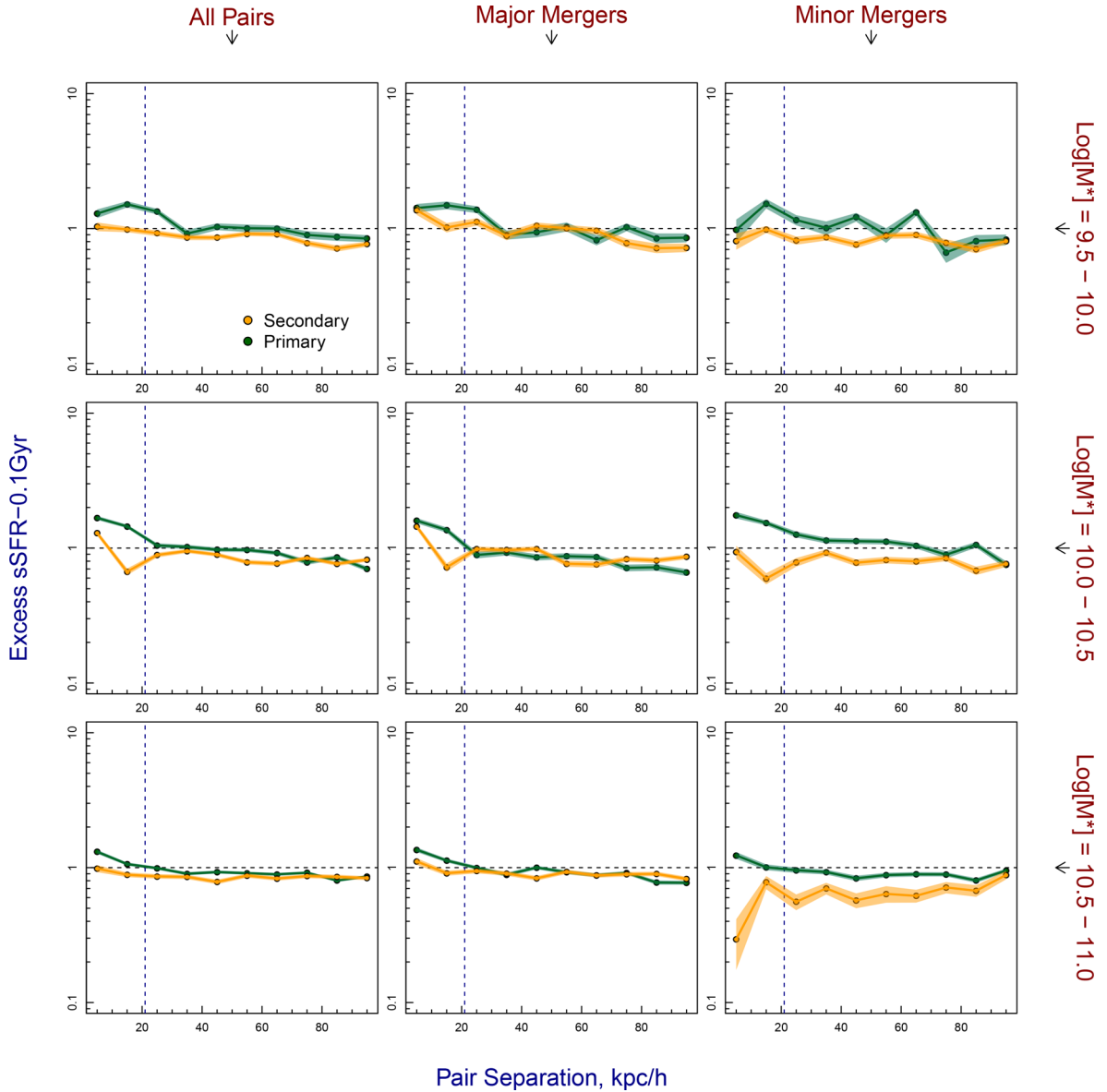
Figure 9. Same as Fig. 6 but for sSFR$_{NUV}$. Green dashed vertical line shows the FWHM of the PSF of *GALEX* NUV at the median redshift of our pair samples. For our SFR$_{FUV}$ indicator, the distributions are almost identical with a slight difference in normalization – as such we do not display both figures.

as a function of pair separation. For all pair galaxies combined (left column), we find increasing SF with deceasing pair separation for both primary and secondary galaxies. Splitting into major and minor mergers, for major mergers we find that primary and secondary galaxies look identical, both have increasing SF with decreasing pair separation. However, for minor mergers we see subtle differences between primary and secondary galaxies. The primary galaxies show a similar relation to those in major mergers, while the secondary galaxies have no enhancement/suppression of SF with pair separation, except for the closest pairs. As with our FIR indicator, there is also a subtle suggestion that the normalization of the secondary galaxies in minor mergers scales as a function of galaxy mass, with higher mass galaxies appearing more suppressed than lower mass galaxies (the orange line is lower in the bottom panel than the top panel of the right column). We do not display both FUV and NUV figures as both

distributions are almost identical, but with slight normalization scaling.

(v) SFR$_{0.1\,Gyr}$ (Fig. 10) – Our SFR$_{0.1\,Gyr}$ measure displays similar results to the SFR$_{NUV}$, but also with a slight normalization change. (This is not surprising as they are all derived from the MAGPHYS fits.) However, for minor mergers and our highest mass bin (bottom-right panel), we now see clear suppression of secondary galaxies at close pair separations.

(vi) SFR$_{H\alpha}$ (Fig. 11) – Here we see the strongest variation in SFRs as a function of pair separation and the most dramatic differences between primary and secondary galaxies in minor mergers. When considering all pairs (left column), we find an increase in SFR for both primary and secondary galaxies (with the enhancement much more dramatic in primary galaxies). This is once again consistent with the results seen in Fig. 5, where Hα-derived SFRs show a strong enhancement of SF when considering close,
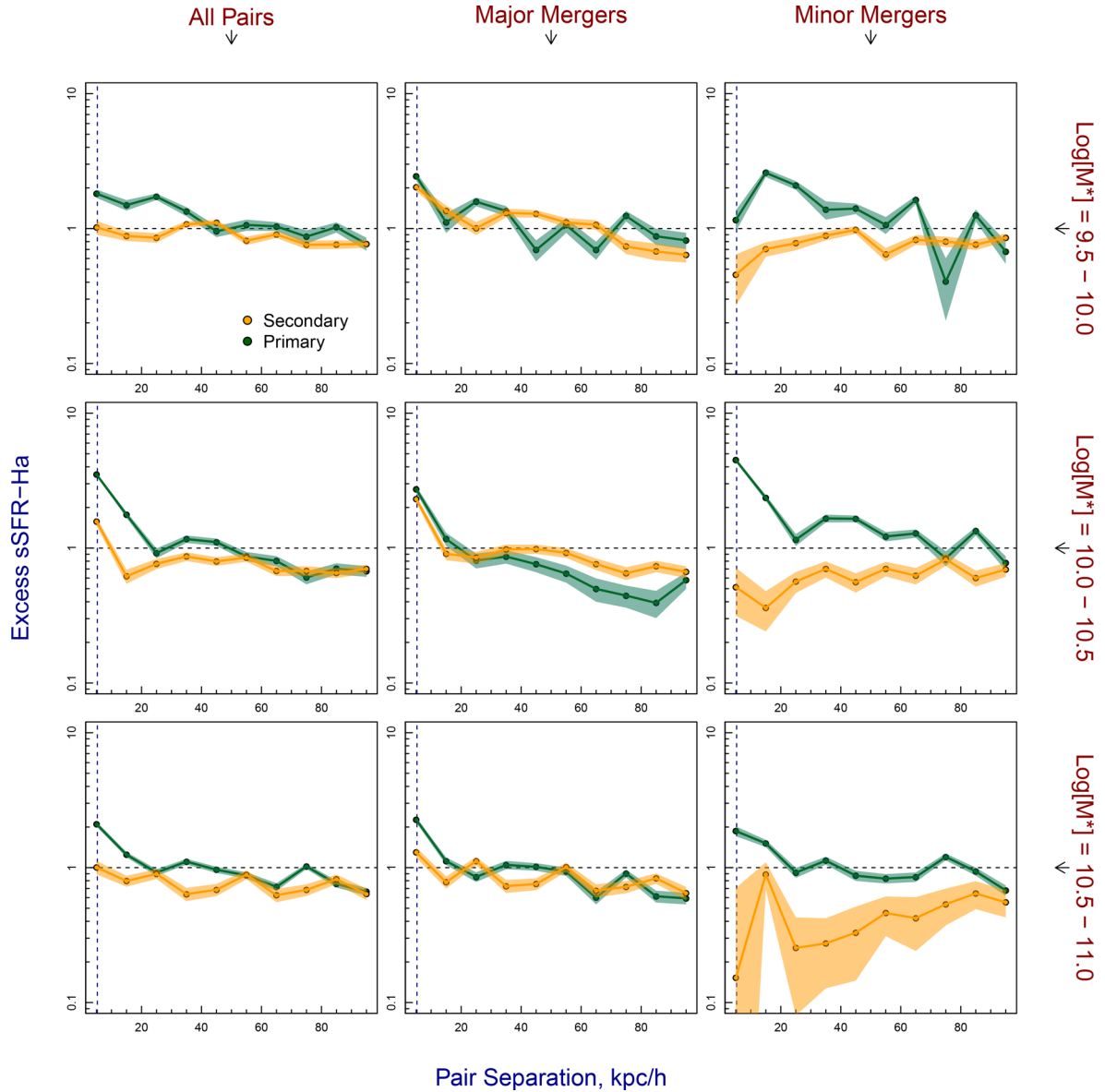
Figure 10. Same as Fig. 6 but for sSFR$_{0.1\,\mathrm{Gyr}}$. Green dashed vertical line shows the FWHM of the PSF of *GALEX* NUV at the median redshift of our pair samples – this band is the main driver of SFR calculated using MAGPHYS.

intermediate and far pairs. However, when we consider just pair galaxies in minor mergers (right column), we see a dramatic change in the SFR with regard to primary/secondary status. Primary galaxies still have their SF strongly enhanced, while secondary galaxies show strong suppression of SF, even at large pair separations (out to $\sim r_{\mathrm{sep}} > 90\,\mathrm{kpc}\ h^{-1}$). This highlights that SF is suppressed in the secondary galaxies of minor mergers. As SFR$_{\mathrm{H}\alpha}$ measures SFRs on the shortest time-scales, it is likely that the enhancement and suppression seen in primary and secondary galaxies, respectively, is a direct consequence of the galaxy interactions. We remind the reader that our Hα flux measurements are not subject to measurement errors from confusion between close pairs, and as such are not systematically biased by errors in flux distribution. Another possible explanation for the trends seen in Hα is that the distribution of star-forming regions within a galaxy changes during the interaction. The recent simulations of Moreno et al. 2015 show that SF can be

significantly enhanced in the central regions of a galaxy during an interaction, but is largely suppressed in its outer parts. As our Hα observations only probe the central regions (due to the aperture-based spectroscopy), we may only be witnessing centrally concentrated suppression/enhancement of SF which is not a true representation of the global effects of the interaction. However, the trends seen in our Hα SFRs are consistent with those in our other short-duration SFR indicators, albeit at a higher significance. Further investigation into the spatial distribution of Hα SF in a subsample of our interacting galaxy sample is underway, and will be the subject of an upcoming paper.

(vii) Global observation – An interesting additional global observation (as alluded to previously) is that pair galaxies appear to become more suppressed in SF as a function of increasing stellar mass. This can be seen in all figures in that the lines systematically drop to lower excess sSFR from the top to bottom panels,

Figure 11. Same as Fig. 6 but for sSFR$_{H\alpha}$. Green dashed vertical line shows the physical size of a 2 arcsec aperture at the median redshift of our pair samples.

and suggests that SF in pair galaxies is not only affected by pair mass ratio and primary/secondary status, but also individual galaxy mass.

4.2.1 Summary of key observables in this section

In summary, we find that the primary galaxies in both major and minor mergers show consistent trends of enhanced SF over our control sample as a function of decreasing pair separation, and that this enhancement is more pronounced in the short-duration SFR indicators of SFR$_{H\alpha}$, SFR$_{FUV/NUV}$ and SFR$_{0.1\,Gyr}$. In contrast, the SF in secondary galaxies shows different characteristics depending on pair mass ratio. In major mergers SF is enhanced at close pair separations, and follows the primary galaxies, while in minor mergers, we see the converse, that secondary galaxies appear to be suppressed at

close pair separations. This effect is also more pronounced for short time-scale SFR indictors. We find that at large pair separations ($r_{sep} > 60\,kpc\ h^{-1}$), pair galaxies look similar in their SFR characteristics, and as such we are likely to be probing these systems prior to significant effects of the interaction. However, we see significant modifications to SFRs at close pair separations, suggesting that the effect is due to the interaction. We also find that the normalization of the distributions in Figs 6–11 marginally drops as a function of stellar mass, which potentially indicates that individual galaxy mass also has an impact on how interactions modify SF.

What is clear from this analysis is that both primary and secondary status within the pair and pair mass ratio play an important role in the modification of SFRs in interactions and we most clearly see the effect of these parameters when measuring SFRs on short time-scales.
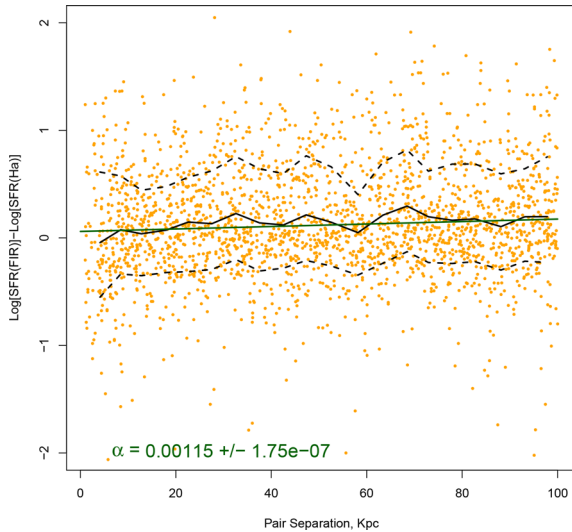
Figure 12. $\log_{10}[\text{SFR}_{\text{FIR}}]$–$\log_{10}[\text{SFR}_{\text{H}\alpha}]$ for our pair sample as a function of pair separation. Black lines show the running median (solid) with upper and lower quartiles (dashed). The green solid line displays the HYPERFIT fit to the median binned distribution (with slope, α). While marginal we see a slight trend in $\log_{10}[\text{SFR}_{\text{FIR}}]$–$\log_{10}[\text{SFR}_{\text{H}\alpha}]$, suggesting that when considering all pair galaxies together, SF may be enhanced on short time-scales in closely interacting pairs.

5 COMPARISONS OF SFR INDICATORS TO PROBE SF ON DIFFERENT TIME-SCALES

In this section, we take our analysis further and combine the effects of both pair separation and SFR indicator time-scale. We also use this analysis to highlight the key differences between primary and secondary galaxies, and major and minor mergers discussed above.

5.1 Scatter in the SFR$_{\text{H}\alpha}$ versus SFR$_{\text{FIR}}$ relation

Prior to a more sophisticated analysis, and as alluded to earlier, Fig. 3 highlights a possible avenue for exploring SFRs in close pairs using multiple SFR indicators. The SFR$_{\text{H}\alpha}$ versus SFR$_{\text{FIR}}$ relation in Fig. 3 displays large scatter with significant offset between Hα- and FIR-derived values for a large number of sources. As the SFR$_{\text{FIR}}$ probes a much longer time-scale than SFR$_{\text{H}\alpha}$, could this highlight short time-scale changes in SF for pair galaxies?

In Fig. 12, we show the offset between $\log_{10}[\text{SFR}_{\text{FIR}}]$ and $\log_{10}[\text{SFR}_{\text{H}\alpha}]$ for pair galaxies as a function of pair separation. The black lines in Fig. 12 display the running median (solid) and upper and lower quartiles (dashed). The green solid line displays the HYPERFIT fit to the median binned values, with slope, α, displayed on the plot. While only marginal, we do see a slight trend between $\log_{10}[\text{SFR}_{\text{FIR}}]$ and $\log_{10}[\text{SFR}_{\text{H}\alpha}]$ as a function of pair separations. Galaxies at large pair separations have slightly larger $\log_{10}[\text{SFR}_{\text{FIR}}]$ than $\log_{10}[\text{SFR}_{\text{H}\alpha}]$, while at small pair separations, the inverse is true. This alludes to the fact the SF, as measured by Hα line emission, is very marginally enhanced over that measured from the FIR continuum for close pairs – potentially highlighting that the enhancement of SF occurs on time-scales of <100 Myr. However, the Spearman's rank correlation coefficient for $\log_{10}[\text{SFR}_{\text{FIR}}]$–$\log_{10}[\text{SFR}_{\text{H}\alpha}]$ against pair separation is just 0.0929, indicating that there is little statistical correlation between the two variables. We shall investigate this potential correlation using a more sophisticated method in the following section.
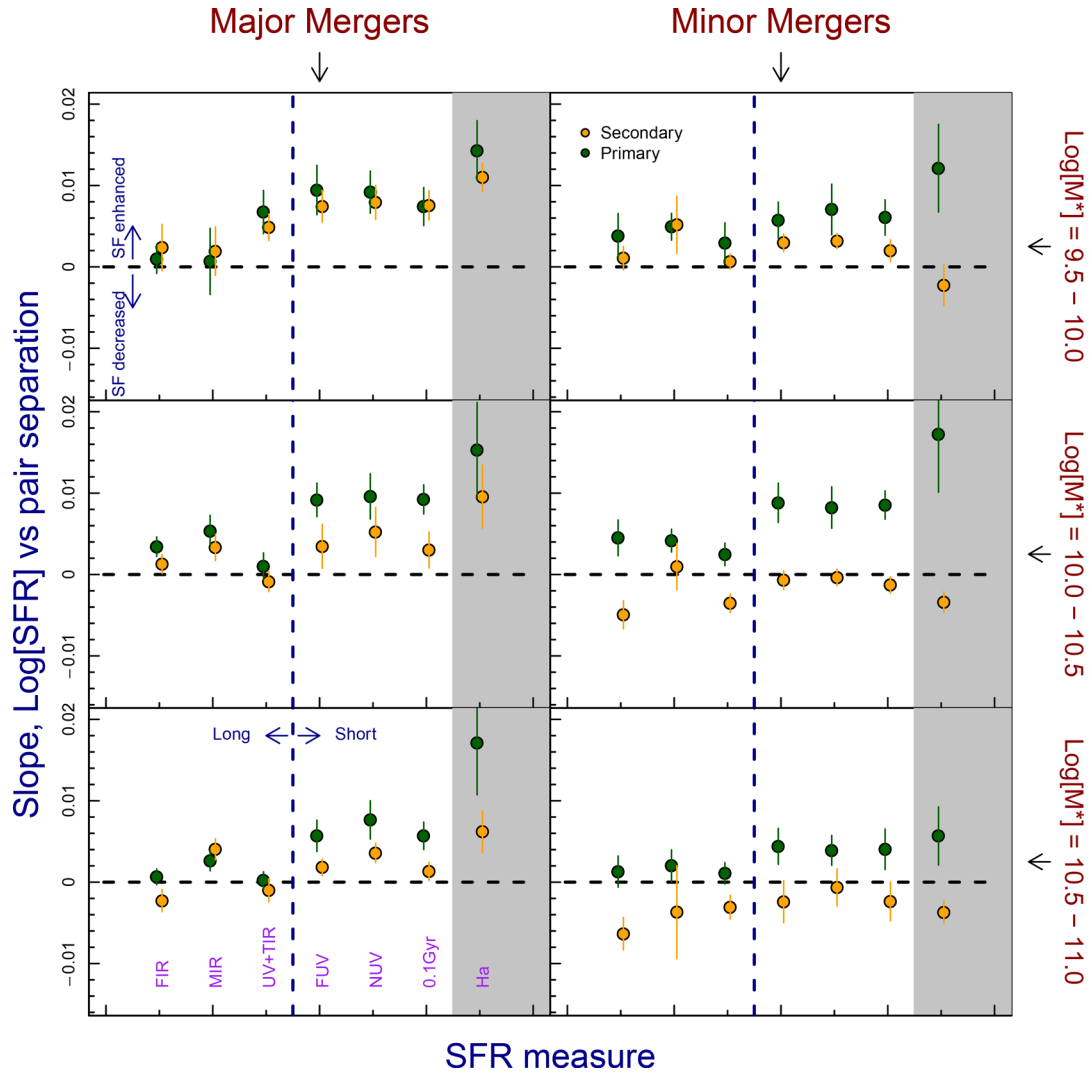
5.2 Direct comparison of all SFR indicators

Taking this further, in this section we compare all of our SFR indicators directly and discuss the implications of variations between each measure. In order to make this comparison, we use the slope of the sSFR versus pair separation relations in Figs 6–11 over the full 100 kpc separation range. We once again use the HYPERFIT package to fit the slope of each pair separation binned distribution and give 1σ errors. While the distributions in Figs 6–11 may not be well fitted by a straight line, we stick to this simple model to avoid complication, and to highlight the general trend of increasing/decreasing excess SF as a function of pair separation.

In Fig. 13, we show the HYPERFIT slope for all SFR indicators split by stellar mass, major/minor mergers and primary/secondary status. The vertical blue dashed line separates long- (>100 Myr) and short-duration (<100 Myr) SFR indicators, as defined earlier in this work. We also highlight the Hα-derived SFR slope in the grey shaded region, noting that this point is derived from nebular emission line measurements from aperture-based spectroscopy, and as such is subject to different biases to our continuum-derived SFRs. The dashed horizontal line displays the dividing line between positive and negative slopes; this highlights either enhancement (slope increasing to smaller pair separations) or suppression (slope decreasing to smaller pair separations) of SF in the interaction in comparison to the most distant pairs (i.e. do close pairs show more or less excess SF than distant pairs?). As such, any significant deviation from zero slope displays that the interaction is affecting SF for that particular sample. We note here again that we also fit these distributions outside of the PSF scale for the main photometric band used in the analysis (blue vertical dashed lines in Figs 6–11), and find that the correlations hold true – but at a less significant level.

Comparing the slopes of the distribution as a function of SFR indicator, we see some interesting trends. First, considering just galaxies in major mergers, we find that as we move to SFR indicators that probe shorter time-scales, SF is enhanced more strongly (for long-duration measures there is no SF enhancement, while for short-duration measures we see consistent enhancement of SF). This is true for both primary and secondary galaxies. It is also interesting to note that once again there appears to be a weak trend with stellar mass; however, this is only apparent in secondary galaxies, with secondary galaxies being less enhanced at increasing stellar mass (the orange points drop from the top to bottom panels). In contrast for galaxies in minor mergers, we find that primary and secondary galaxies show different characteristics. Primary galaxies display similar trends to the primary galaxies in major mergers, showing excess SF for short-duration measures. Secondary galaxies largely show suppression of SF, in all but the smallest mass bin. What is clear from this figure is that for short-duration SFR indicators, secondary galaxies in minor mergers show different characteristics from their primary counterparts.

These results are indicative of SF being enhanced in primary galaxies of all mergers and secondary galaxies being enhanced in major mergers and suppressed in minor mergers, but only when measured on short time-scales.

To highlight the dependence on primary/secondary status and pair mass ratio of the modification of SFRs in interactions further, we compare differences between the slopes for major and minor mergers, at fixed stellar mass binning and pair status (Fig. 14) and differences between primary and secondary galaxies at fixed pair mass ratio (Fig. 15). Error bars in these figures are derived from the sum of the squares of the HYPERFIT errors given in Fig. 13. In
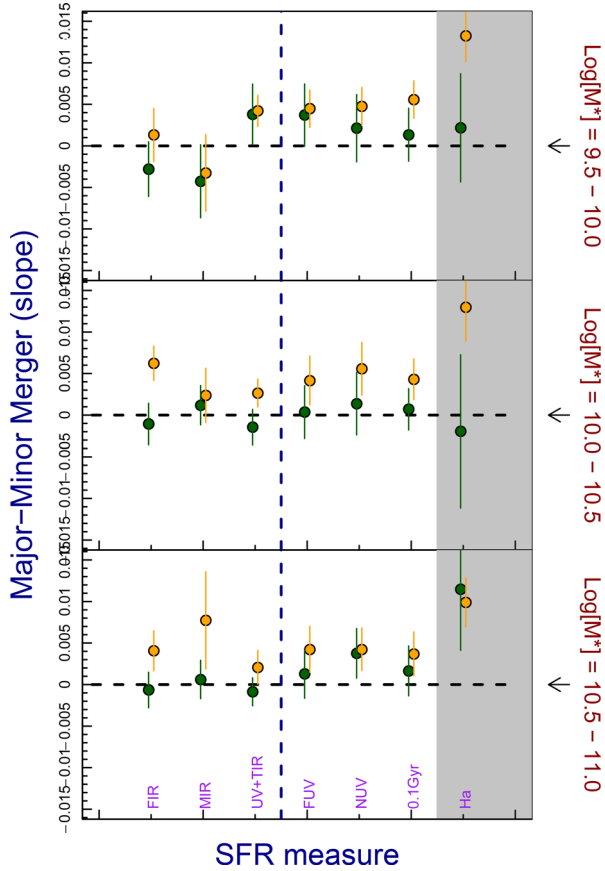
Figure 13. Comparison of the slopes of $\log_{10}$[sSFR] versus pair separation for all SFR indicators shown in Fig. 6–11. Samples are split by stellar mass (rows) and pair mass ratio (columns), as well as primary (green) and secondary (orange) status within the pair. We divide SFR indicators into long and short duration with the vertical blue dashed line, and highlight the Hα emission line-derived SFR with the grey shaded region. Significant deviations from the central horizontal line display modifications to SF induced by the a merger – positive values display enhancement of SF and negative values suppression of SF. Error bars display the 1σ error on the HYPERFIT fit to the slope.

Fig. 14, offsets from the central line display a significant difference in the effect of interactions between major and minor mergers, where positive values show that SF is more strongly suppressed in a minor merger. Note that this figure does not show absolute values and as such zero does not highlight that there is no change to SFRs in the interaction, only that there is *no difference* between major/minor mergers galaxies. We find that primary galaxies are largely consistent with their being no difference between major and minor mergers for all SFR indicators (the green points are largely consistent with the central line given the errors), while the secondary galaxies stronger suppression of SF in minor mergers than major mergers (the orange points lie above the central line). This effect appears largest in short-duration SFR indicators (i.e. the differences between secondary galaxies in major and minor mergers are most apparent when probed on short time-scales).

In Fig. 15, offsets from the central line display a significant difference in the effect of interactions between primary and secondary galaxies, where positive values show that SF is more strongly sup-

pressed in the secondary galaxy. We find that for major mergers there is little difference between primary and secondary galaxies specifically for long-duration indicators (as discussed previously). We do see that for short-duration time-scale indicators, secondary galaxies are marginally suppressed in comparison to primary galaxies when considering the higher stellar mass bins only (the golden and purple triangles lie above the central line), but this effect is small. For minor mergers, we see a larger discrepancy between primary and secondary galaxies. Secondary galaxies appear to be suppressed relative to primaries for all SFR indicators and in the majority of stellar mass bins (the majority of points in the right-hand panel of Fig. 15 lie above the central line). This effect also appears to be more pronounced for short-duration indicators and at intermediate stellar masses.

In combination, these figures highlight that the secondary galaxies in minor mergers show distinctly different SF characteristics from all other pair galaxies, but this effect is only strong when SFRs are measured on <100 Myr time-scales.

Figure 14. Comparison of the difference of the $\log_{10}$[sSFR] versus pair separation slope between major and minor mergers. Values given are the offset between corresponding points in the left and right columns in Fig. 13. Significant offsets from the central line show differences between major and minor mergers for each population and SFR indicator. Once again, secondary galaxies show more significant differences between major and minor mergers.

6 SUMMARY OF THE EFFECT OF CLOSE INTERACTIONS ON GALAXY SFRS AND DISCUSSION

Now we outline the key results outlined in the previous two sections and discuss a possible toy model for SF in galaxy mergers which may explain these results.

(i) Considering pair populations as a whole, SF can appear either unaffected or enhanced by an interaction depending on the SFR indicator used (Fig. 5).

(ii) At large pair separations (>50 kpc), we see little difference between different galaxy populations, suggesting that these systems are not being strongly affected by the interaction (Figs 6–11).

(iii) At close pair separations (<30 kpc), we see both enhancement and suppression of galaxy SFRs depending on the subsample of galaxies we select, and this modification to SFRs appears more strongly for short-duration SFR indicators (Figs 6–11).

(iv) For long time-scale SFR indicators, we see little enhancement or suppression of SF in interacting galaxies. This holds true for both major and minor mergers, and for both primary and secondary galaxies – suggesting that we are probing the SF in the galaxy prior to its SFR being modified by the interaction (Fig. 13).

(v) For short time-scale SFR indicators (especially Hα), primary galaxies show enhancement in SF at close pair separations, which is consistent across major and minor mergers (Fig. 13).

(vi) For short time-scale SFR indicators, secondary galaxies show distinctly different characteristics between major and minor mergers. In major mergers, SF is enhanced with decreasing pair separation, while in minor mergers SF is suppressed with decreasing pair separation (Figs 13–15).

(vii) Primary galaxies appear largely agnostic to pair mass ratio while secondary galaxies show suppression in minor mergers only (Figs 13–15).

To relate these observables to the true effects of interactions on SFRs, we use both the pair separation and variation of SFR indicators on different time-scales as a proxy for the stage of the galaxy interaction. We relate both our long-duration SFR indicators at all
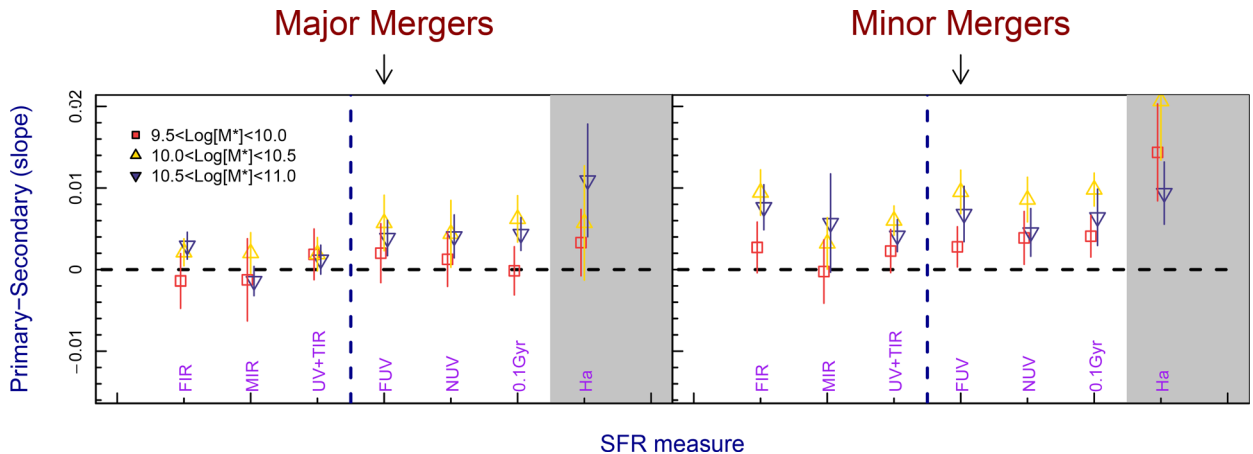
Figure 15. Comparison of the difference of the $\log_{10}$[sSFR] versus pair separation slope between primary and secondary galaxies. Values given are the offset between primary and secondary galaxies in each row in Fig. 13. Significant offsets from the central line show differences between primary and secondary galaxies at each stellar mass and SFR indicator. Once again, secondary galaxies in minor mergers show more significant differences between primary and secondary galaxies, specifically for short-duration SFR indicators.
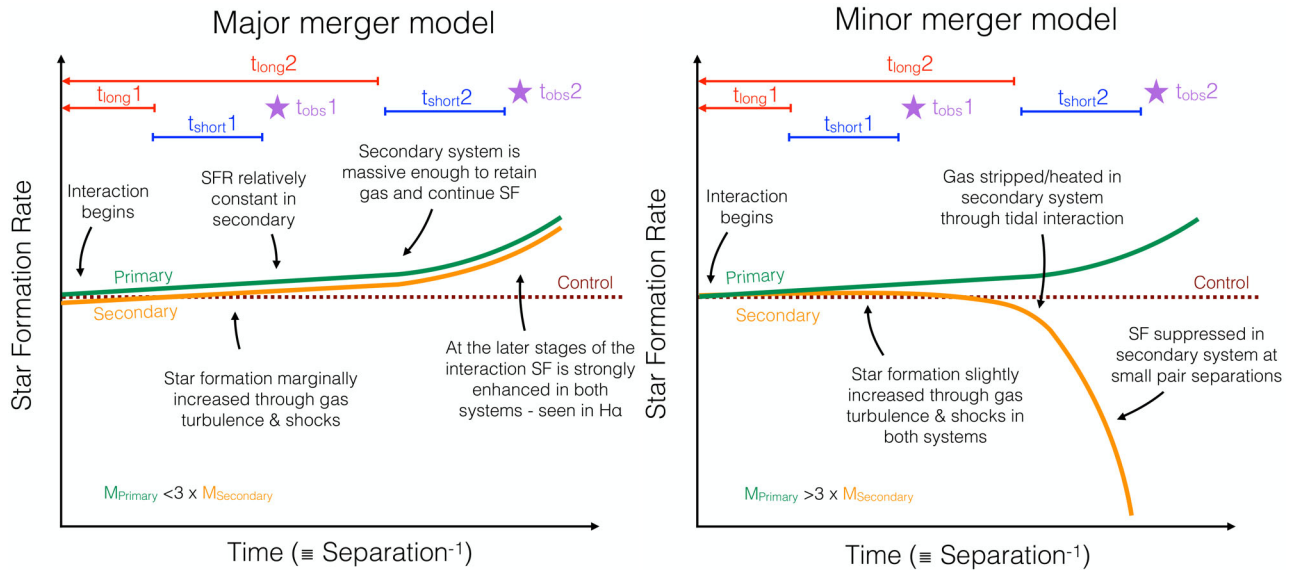
Figure 16. A toy model for the evolution of SF in major (left) and minor (right) merger systems. The purple stars highlight two possible observation epochs during the merger. These are proceeded by the likely time-scales over which long-duration and short-duration SFRs are measured at each epoch (red and blue horizontal bars, respectively – note that red bars would extend off the left edge of the plot). These models are consistent with our observations of SF in pair systems and can potentially explain the seemingly contradictory previously obtained results for SF in close pairs as SF is enhanced in all merger scenarios, except in the secondary galaxy in minor mergers at close separation. As such, our measure of how SF is affected in galaxy interaction is dependent on pair mass ratio and primary/secondary status within the pair.

separations and our short-duration measures at large pair separations to be representative of the pre-, or early-interaction stage. Conversely, our short-duration measures at close pair separations are representative of the late-interaction stage. This simplistic model assumes that all galaxies are on their first approach and that they have not had previous passes, which would affect their SF. Such systems could reach relatively large pair separations, but would have already had their SF enhanced/suppressed by the interaction. In our analysis, we have no method of determining if galaxies have already had one or more passes prior to the observation epoch, as such we cannot account for this affect. However, we note that Robotham et al. (2014) find that, for the pair sample used in this work, galaxies at $r_{sep} < 20$ kpc show much greater signs of visual disturbance than those at $20 < r_{sep} < 50$ kpc and both these populations show higher visual disturbance than pairs at $r_{sep} > 50$ kpc. This indicates that galaxies are more strongly affected by interactions at closer separations, and while a fraction of galaxies at large separations may have already had a number of passes, the major trend is that closer separations mean stronger pair interactions and a later stage in the merger process. Therefore, we deem it is reasonable to assume that to first order pair separation can be directly related to merger time-scale.

Using these assumptions, we can piece together a hypothetical toy model for SF in the primary and secondary galaxies in both major and minor merger systems. Fig. 16 displays this hypothetical model with interaction time/pair separation plotted against current SFR. We also display the time-scales over which both long- and short-duration SFRs are measured, for two different scenarios: t1, when the galaxies are at large pair separations (an early stage in their interaction) and t2, when the galaxies are at small pair separations (a late stage in their interaction).

In our major merger model, SF remains relatively constant throughout the merger in both the primary galaxy and secondary galaxy, but is enhanced at the very late stages (we see the strongest

enhancement in the shortest time-scale indicator – Hα). These enhancements in SF are likely to be due to gas turbulence, tidal torques or shocks caused by the gravitational attraction of the other system. In this scenario, the secondary galaxy has sufficient mass (in comparison to the primary) to retain its gas and continue star-forming at a relatively constant rate, i.e. it is not tidally stripped. This is consistent with our observations summarized above. The primary and secondary galaxies show some enhancement of SF with pair separation, and this increases for the shortest time-scale indicator. If SFRs were measured at t1 and t2, we would observe a marginally increasing measure of both long- and short-duration SFRs (the primary and secondary galaxies show similar SF properties which increase in SF for short-duration measures). The largest tidal interaction will occur at the smallest pair separation and be most evident in the shortest duration SFR indicator, and as such we see the largest enhancement of SF in Hα-derived SFRs.

For our minor merger model, the primary galaxy follows the same SF evolution as both systems in the major merger. It is sufficiently high mass in comparison to the secondary to retain its gas and continue star-forming, and has its SFR enhanced over time as interactions with the secondary systems cause gas turbulence and shocks. However, the secondary system follows a different SF evolution path during the interaction. Initially its SF is not significantly altered and hence we do not see distinct differences in long-duration SFR measures or large pair separations, which probe this epoch. However, at some stage during the interaction, SF begins to be suppressed. This is likely through tidal stripping or gas heating. This is evident as the suppressed SFRs at close pair separations and in short-duration SFR indicators. If we were to measure the SFR of the secondary system at t1 and t2, we would find that at t1 (large separation), the galaxy would look somewhat like the primary galaxy, and we would see no suppression of SF. However, at t2 we would find short-duration SFRs suppressed relative to t1; this effect would

not yet be observable in the long-duration SFR measures. At this point, the secondary galaxy SFRs would be distinctly different from the primary galaxy when observed using short-duration indicators – this model is also consistent with the observations summarized above.

If representative of the true galaxy–galaxy interactions, these toy models could potentially explain the contradictory results from previous studies which find both SF enhancement and suppression in close pair systems. Our models predict that SF is enhanced in the majority of cases – where mass ratios are close to 1:1, as well as in the primary galaxy in a minor merger. However, SF is suppressed in the secondary galaxy in minor mergers, but only at close pair separations. As such, whether SF is enhanced or suppressed in galaxy–galaxy interactions is largely dependent on the pair mass ratio and pair separation. Clearly by observing galaxies at different interaction stages and at different pair mass ratios, we will obtain conflicting results as to the suppression/enhancement of SF in interacting systems.

7 CONCLUSIONS

We have investigated SF activity as a function of pair separation for interacting galaxies for different merger scenarios, using SFRs derived from multiple SFR indicators covering a range of time-scales. The key results from our analysis are as follows.

(i) SF in interactions proceeds differently for galaxies in minor mergers than in major mergers.

(ii) SF in minor mergers proceeds differently in galaxies depending on whether they are the primary (high-mass) or secondary (low-mass) galaxy.

(iii) Primary galaxies show some enhancement of SF in all mergers which is only evident for the shortest time-scales – and as such the later stages of the interaction.

(iv) Secondary galaxies show little change in SF in major mergers, except for some enhancement on the shortest time-scales, but are suppressed in minor mergers.

(v) SF suppression in secondary galaxies occurs on time-scales of $\lesssim 100$ Myr as it is not evident in long-duration SFR measures – as such, it also occurs at a late stage in the interaction.

Using these results we propose a scenario for the evolution of SF in major and minor merger systems. In the major mergers, both primary and secondary galaxies have their SF marginally enhanced through tidal turbulence and shocks for the early stages. At the later stages of the merger, SF is likely to be enhanced. SF is not suppressed as both galaxies have sufficient mass (in relation to the other) to retain their gas. In the minor mergers, the primary galaxy follows the same SF enhancement as the major merger systems, while the secondary galaxy has its SF suppressed as its gas is either tidally stripped, heated or simply stretched to a lower mean density which is not sufficient for SF. This toy model is consistent with the recent findings of Robotham et al. 2013 and De Propris et al. 2014, as well as the galaxy merger simulation of Di Matteo et al. 2007 – predicting that the effects of galaxy interactions on SF are dependent on both pair mass ratio and primary/secondary status within the pair.

ACKNOWLEDGEMENTS

REFERENCES

Baldry I. K. et al., 2010, MNRAS, 404, 86
Baldwin J. A., Phillips M. M., Terlevich R., 1981, PASA, 93, 5
Barro G. et al., 2011, ApJS, 193, 30
Bell E. F. et al., 2005, ApJ, 625, 23
Bournaud F., Powell L. C., Chapon D., Teyssier R., 2011, in Brummell N., Brun A. S., Ponty Y., Miesch M. S., eds, Proc. IAU Symp. 271, Astrophysical Dynamics: From Stars to Galaxies. Cambridge Univ. Press, Cambridge, p. 160
Bourne N. et al., 2012, MNRAS, 421, 3027
Brown M. J. I. et al., 2014, ApJS, 212, 18
Calzetti D. et al., 2007, ApJ, 666, 870
Casteels K. R. V. et al., 2014, MNRAS, 445, 1157
Chabrier G., 2003, PASP, 115, 763
Chary R., Elbaz D., 2001, ApJ, 556, 562
Cluver M. E. et al., 2014, ApJ, 782, 90
Conselice C. J., 2014, ARA&A, 52, 291
Conselice C. J., Bershady M. A., Dickinson M., Papovich C., 2003, AJ, 126, 1183
Conselice C. J., Blackburne J. A., Papovich C., 2005, ApJ, 620, 564
da Cunha E., Charlot S., Elbaz D., 2008, MNRAS, 388, 1595
Davé R., 2008, MNRAS, 385, 147
Davies J. I. et al., 2014, MNRAS, 438, 1922
De Propris R. et al., 2014, MNRAS, 444, 2200
de Ravel L. et al., 2009, A&A, 498, 379
Di Matteo P., Combes F., Melchior A.-L., Semelin B., 2007, A&A, 468, 61
Driver S. P. et al., 2011, MNRAS, 413, 971
Driver S. P., Robotham A. S. G., Bland-Hawthorn J., Brown M., Hopkins A., Liske J., Phillipps S., Wilkins S., 2013, MNRAS, 430, 2622
Eales S. et al., 2010, PASP, 122, 499
Ellison S. L., Patton D. R., Simard L., McConnachie A. W., 2008, AJ, 135, 1877
Freedman Woods D., Geller M. J., Kurtz M. J., Westra E., Fabricant D. G., Dell'Antonio I., 2010, AJ, 139, 1857
Gilbank D. G., Baldry I. K., Balogh M. L., Glazebrook K., Bower R. G., 2010, MNRAS, 405, 2594
Gunawardhana M. L. P. et al., 2011, MNRAS, 415, 1647
Hopkins P. F., Hernquist L., Cox T. J., Kereš D., 2008, ApJS, 175, 356
Hopkins A. M. et al., 2013, MNRAS, 430, 2047
Kauffmann G. et al., 2003, MNRAS, 346, 1055
Kazantzidis S. et al., 2005, ApJ, 623, L67
Kennicutt R. C., Jr, 1998, ApJ, 498, 541
Kennicutt R. C., Evans N. J., 2012, ARA&A, 50, 531
Kewley L. J., Maier C., Yabe K., Ohta K., Akiyama M., Dopita M. A., Yuan T., 2013, ApJ, 774, L10
Lewis I. J. et al., 2002, MNRAS, 333, 279
Li C., Kauffmann G., Heckman T. M., Jing Y. P., White S. D. M., 2008, MNRAS, 385, 1903
Lin L. et al., 2008, ApJ, 681, 232
López-Sánchez Á. R., 2010, A&A, 521, A63

López-Sánchez Á. R., Koribalski B. S., van Eymeren J., Esteban C., Kirby E., Jerjen H., Lonsdale N., 2012, MNRAS, 419, 1051

Lotz J. M., Jonsson P., Cox T. J., Primack J. R., 2008a, MNRAS, 391, 1137

Lotz J. M. et al., 2008b, ApJ, 672, 177

Lotz J. M., Jonsson P., Cox T. J., Primack J. R., 2010, MNRAS, 404, 590

Medling A., U, V. Guedes J., Max C. E., Mayer L., 2013, American Astronomical Society Meeting Abstracts, Vol. 221, p. 405.03

Melbourne J. et al., 2012, ApJ, 748, 47

Meurer G. R., Heckman T. M., Calzetti D., 1999, ApJ, 521, 64

Moreno J., Torrey P., Ellison S. L., Patton D. R., Bluck A. F. L., Bansal G., Hernquist L., 2015, MNRAS, 448, 1107

Mortlock A. et al., 2013, MNRAS, 433, 1185

Owers M. S., Blake C., Couch W. J., Pracy M. B., Bekki K., 2007, MNRAS, 381, 494

Papovich C. et al., 2007, ApJ, 668, 45

Patton D. R., Torrey P., Ellison S. L., Mendel J. T., Scudder J. M., 2013, MNRAS, 433, L59

Popescu C. C., Misiriotis A., Kylafis N. D., Tuffs R. J., Fischera J., 2000, A&A, 362, 138

Robotham A. et al., 2010, PASA, 27, 76

Robotham A. S. G. et al., 2011, MNRAS, 416, 2640

Robotham A. S. G. et al., 2012, MNRAS, 424, 1448

Robotham A. S. G. et al., 2013, MNRAS, 431, 167

Robotham A. S. G. et al., 2014, MNRAS, 444, 3986

Rudnick G. et al., 2003, ApJ, 599, 847

Saunders W. et al., 2004, Proc. SPIE, 5492, 389

Sauvage M., Tuffs R. J., Popescu C. C., 2005, Space Sci. Rev., 119, 313

Scudder J. M., Ellison S. L., Torrey P., Patton D. R., Mendel J. T., 2012, MNRAS, 426, 549

Sharp R. et al., 2006, Proc. SPIE, 6269, 62690G

Shi Y., Rieke G., Lotz J., Perez-Gonzalez P. G., 2009, ApJ, 697, 1764

Taylor E. N. et al., 2009, ApJS, 183, 295

Taylor E. N. et al., 2011, MNRAS, 418, 1587

Ueda J. et al., 2012, ApJ, 745, 65

Ueda J. et al., 2013, in Kawabe R., Kuno N., Yamamoto S., eds, ASP Conf. Ser. Vol. 476, New Trends in Radio Astronomy in the ALMA Era. Astron. Soc. Pac., San Francisco, p. 61

Villforth C. et al., 2014, MNRAS, 439, 3342

Wang B., Heckman T. M., 1996, ApJ, 457, 645

White S. D. M., Frenk C. S., 1991, ApJ, 379, 52

Wijesinghe D. B. et al., 2011, MNRAS, 410, 2291

Wilkins S. M., Gonzalez-Perez V., Lacey C. G., Baugh C. M., 2012, MNRAS, 427, 1490

Wong K. C. et al., 2011, ApJ, 728, 119

Xilouris E. M. et al., 2012, A&A, 543, A74

Zehavi I. et al., 2011, ApJ, 736, 59

APPENDIX A: ROBOTHAM ET AL. SAMPLE SPLIT BY MAJOR/MINOR MERGER AND PRIMARY/SECONDARY STATUS

In Fig. A1, we display the pair sample of Robotham et al. (in preparation) discussed in Section 4 but split into major/minor mergers and primary/secondary status. These distributions echo the main results derived in this paper. Considering the populations as a whole, we see enhancement of SF in close pairs, but this enhancement is only observable in SFR indicators which probe short time-scales. Splitting the samples into primary and secondary galaxies, we find that the increase in SF for close pairs is completely driven by the primary galaxies, where strong excess is seen for short-duration indicators (specifically Hα). Splitting further based on both pair mass ratio and galaxy status, we find that it is the primary galaxies in both major and minor mergers that show strong enhancement in SF. For secondary galaxies, we see little difference between far, intermediate and close pairs for all SFR indicators. This is consistent with the main results in this paper, when derived in a separate, but complementary, manner.
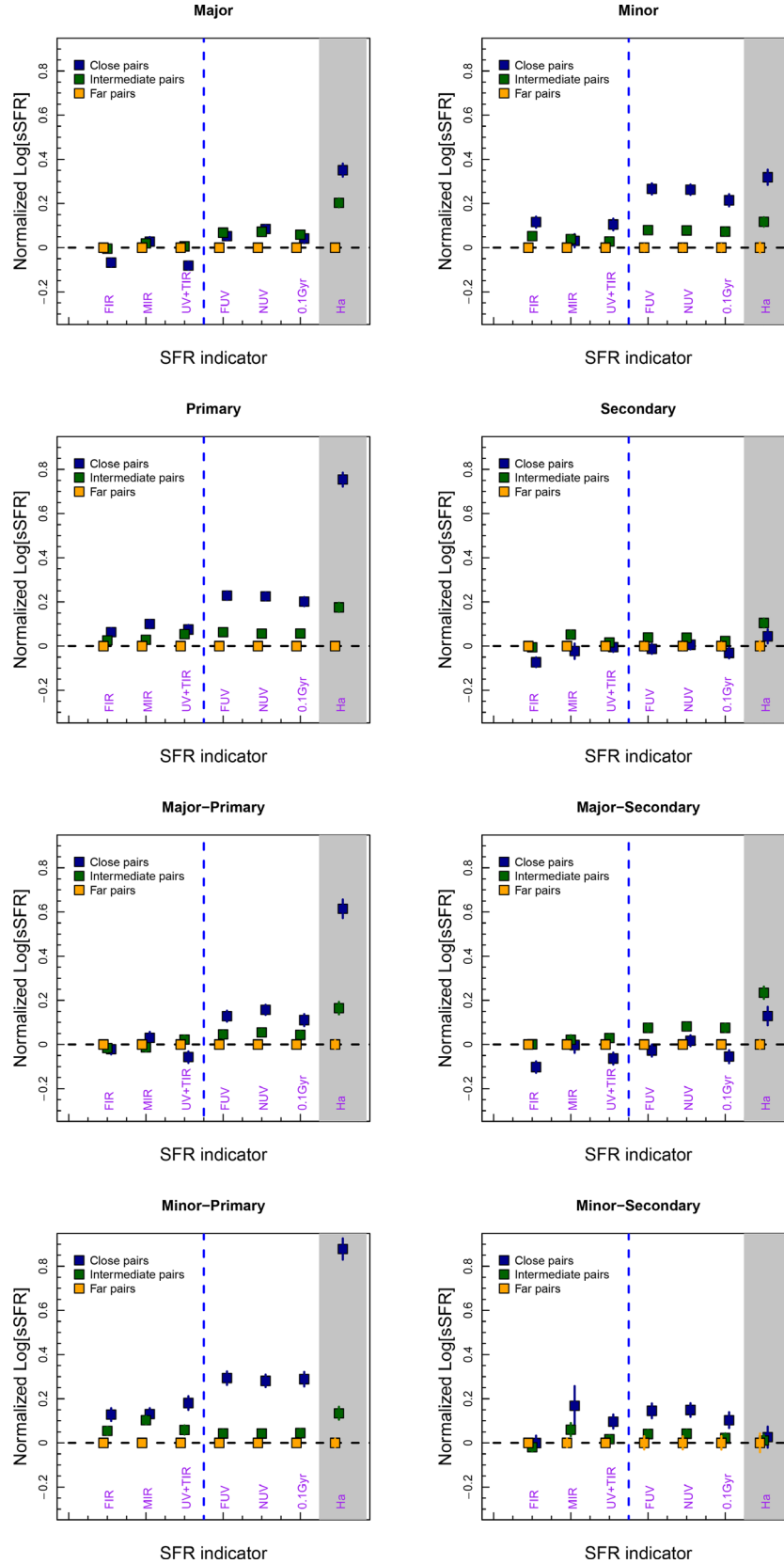
Figure A1. Pair galaxies selected from Robotham et al. (in preparation) split by major/minor mergers and primary/secondary status. All pair samples are normalized to the far pairs' value to highlight the effects of interactions on pair galaxies in each SFR indicator.

[1]*ICRAR, The University of Western Australia, 35 Stirling Highway, Crawley, WA 6009, Australia*

[2]*SUPA, School of Physics and Astronomy, University of St Andrews, North Haugh, St Andrews, Fife, KY16 9SS, UK*

[3]*NASA Ames Research Centre, N232, Moffett Field, Mountain View, CA 94035, USA*

[4]*Astrophysics Research Institute, Liverpool John Moores University, IC2, Liverpool Science Park, 146 Brownlow Hill, Liverpool L3 5RF, UK*

[5]*Sydney Institute for Astronomy, School of Physics A28, University of Sydney, NSW 2006, Australia*

[6]*Australian Astronomical Observatory, PO Box 915, North Ryde, NSW 1670, Australia*

[7]*School of Physics and Astronomy, Monash University, Clayton, VIC 3800, Australia*

[8]*University of the Western Cape, Robert Sobukwe Road, Bellville, Cape Town 7535, South Africa*

[9]*School of Mathematics and Physics, University of Queensland, Brisbane, QLD 4072, Australia*

[10]*Max Planck Institut fuer Kernphysik, Saupfercheckweg 1, D-69117 Heidelberg, Germany*

[11]*Instituto de Astronomía, Universidad Nacional Autónoma de México, A.P. 70-264, 04510 México D.F., Mexico*

[12]*Department of Physics and Astronomy, Macquarie University, NSW 2109, Australia*

[13]*Astronomy Centre, Department of Physics and Astronomy, University of Sussex, Falmer, Brighton BN1 9QH, UK*

[14]*Institute for Computational Cosmology, Department of Physics, Durham University, Durham DH1 3LE, UK*

[15]*Jeremiah Horrocks Institute, University of Central Lancashire, Preston PR1 2HE, UK*

[16]*The Astronomical Institute of the Romanian Academy, Str. Cutitul de Argint 5, Bucharest, Romania*

[17]*Finnish Centre for Astronomy with ESO, University of Turku, Vaisäläntie 20, FI-21500 Piikkiö, Finland*

[18]*Research School of Astronomy & Astrophysics, Mount Stromlo Observatory, Cotter Road, Weston Creek, ACT 2611, Australia*

[19]*SRON Netherlands Institute for Space Research, Landleven 12, NL-9747 AD, Groningen, The Netherlands*

[20]*Department of Physics and Astronomy, University of Canterbury, Private Bag 4800, Christchurch 8140, New Zealand*

[21]*Institute for Astronomy, University of Edinburgh, Royal Observatory, Edinburgh EH9 3HJ, UK*

[22]*School of Physics & Astronomy, Cardiff University, The Parade, Cardiff CF24 3AA, UK*

This paper has been typeset from a TEX/LATEX file prepared by the author.